Extended Speed Range Control of an Open Winding Induction Motor Using a Dual Inverter Drive

by

Saeed Abdullah Wdaan

A thesis submitted in partial fulfillment of the requirements for the degree of

Master of Science

in

Energy Systems

Department of Electrical and Computer Engineering

University of Alberta

Abstract

The dual inverter drive (DID) using an open-ended winding induction machine has been regarded as a suitable topology for high speed applications. Some of the main advantages this topology has over the traditional single inverter drive is its multilevel voltage, its high reliability, and its voltage boost. The DID using a floating capacitor bridge topology has been in existence for a long period, but performance improvement is still possible in terms of its voltage utilization. The aim of this work is to further utilize the capabilities of this topology to improve the operation in the field weakening region.

This topology uses the floating capacitor bridge to supply the motor reactive power demand, whereas the bridge connected to the main power supply is usually operated at unity power factor. This limits the DID operation, especially in the field weakening region where the reactive power supplied to the motor defines the speed range in the field weakening region. The main contribution of this work is to extend the DID's speed range in the field weakening region, improve the motor speed acceleration performance, output power and torque by using the main bridge to supply some reactive power after the floating bridge reaches its maximum limit. It is found that the presented controller can increase the drive's speed extension ratio to 9.2 times the rated speed compared to 5 when always operating the main bridge at unity power factor. The motor maximum fundamental voltage is 1.82 p.u compared to that of a single inverter drive.

Preface

This thesis work is carried out by Saeed Wdaan under the supervision of Dr. John Salmon from the Department of Electrical and Computer Engineering at the University of Alberta. Some parts of this thesis have been published as journal and conference publications and have been reorganized for clear presentation.

Journal

1. **S. Wdaan**, C. Perera and J. Salmon, "Maximum Torque Operation of Open-Winding Induction Motor Dual Drives Using a Floating Capacitor Bridge in the Field Weakening Region," in IEEE Transactions on Power Electronics, vol. 37, no. 8, pp. 9629-9640, Aug. 2022. [**Published**]

Conference

1. **S. Wdaan**, C. Perera and J. Salmon, "Field Weakening Operation of Open-Winding Induction Motor Dual Drives Using a Floating Capacitor Bridge Inverter," 2021 IEEE Energy Conversion Congress and Exposition (ECCE), 2021, pp. 4915-4920. [**Published**]

To my mother, father, brother, sisters, and myself . . .

Acknowledgements

I would like to recognize and thank my supervisor, Dr. John Salmon, first and foremost, for giving me the opportunity to join his research group and for his support, guidance, and expertise throughout my graduate program. I am most grateful for the guidance he provided me and for being very accessible throughout this program period. I have gained an immense amount of knowledge and experience under his supervision.

I am very grateful to my mother and father for being always present in my life and for sharing their wisdom and unique view of the world with me. They have always been there when I needed them. I want to thank my brother and sisters for being supportive and always record and share all family moments with me. This really made me feel home.

I have been very fortunate to have joined this research group, as I have been able to meet a wonderful group of colleagues who, beyond that, I consider my friends. I want to thank Dr. Chatumal for sharing his knowledge and helping me running experiments and speeding up the learning curve and Mr. Marius, who greatly helped me connecting the experimental setup and being supportive during early experimental stages.

Lastly, I would like to thank the National Science and Engineering Research Council of Canada (NSERC), Energy Systems Lab Facilities of University of Alberta, and the Hadhramout Establishment, Yemen, for their funding and monetary support towards my research, without which this thesis would not have been possible.

~ Saeed Wdaan, September 2022

Contents

List of Tables

List of Figures

List of Abbreviations

OEWIM	Open-Ended Winding Induction Machine
DID	Dual Inverter Drive
EVs	Electric Vehicles
IM	Induction Machine
FW	Field Weakening
DC	Direct Current
PWM	Pulse-Width Modulation
MB	Main Bridge
FB	Floating Bridge
FOC	Field Oriented Control
UPF	Unity Power Factor
RFRF	Rotor Flux Reference Frame
SCRF	Stator Current Reference Frame
RPM	Revolutions Per Minute
PI	Proportional Integral
EMF	Electro Motive Force
CMV	Common Mode Voltage
INV	Inverter
PF	Power Factor
p.u.	Per-Unit

List of Symbols

V_{dc}	DC-link voltage of power supply.	V
$\overline{v}_{mb}$	Voltage space vector of MB inverter.	V
$\overline{v}_{fb}$	Voltage space vector of FB inverter.	V
$\overline{v}_s$	Voltage space vector of IM stator.	V
$\bar{i}_s$	Space vector of the stator current.	A
$i_{d,s}$	d-axis component of stator current in rotor flux reference frame.	A
$i_{q,s}$	q-axis component of stator current in rotor flux reference frame.	A
$I_{q,s}$	Rated q-axis component of stator current in rotor flux reference frame.	A
$I_{d,s}$	Rated d-axis component of stator current in rotor flux reference frame.	A
v_d	d-axis component of stator voltage in rotor flux reference frame.	V
v_q	q-axis component of stator voltage in rotor flux reference frame.	V
v_P	Active voltage component in stator current reference frame.	V
v_Q	Reactive voltage component in stator current reference frame.	V
V_{max}	Maximum fundamental phase voltage of inverter.	V
$V_{max,mb}$	Maximum fundamental phase voltage of MB inverter.	V
$V_{max,fb}$	Maximum fundamental phase voltage of FB inverter.	V
I_{max}	Maximum motor phase current.	A
ω_{rated}	Rated electrical motor speed.	rad./s.
ω_r	Electrical rotor speed.	rad./s.
ω_m	Mechanical rotor speed.	rad./s.
ω_{sl}	Slip frequency.	rad./s.
ω_1	Region I speed limit.	rad./s.
ω_2	Region II speed limit.	rad./s.
ω_2/ω_{rated}	Speed extension ratio.	p.u.

T_e	Electromechanical torque.	N_m
P_{mech}	Mechanical output power.	W
P	Real power.	W
Q	Reactive power.	W
$\overline{\varphi}_s$	Stator flux space vector, defined as $\overline{\varphi}_s = L_s(i_d + j\sigma i_q)$.	mT
L_s, L_r, L_m	Stator, rotor, and magnetizing inductances.	mH
σ	Leakage coefficient, defined as $\sigma = 1 - \frac{L_m^2}{L_s L_r}$.	p.u.
θ_{flux}	The phase of the rotor flux reference frame.	deg.
$\theta_{current}$	The phase of the stator current reference frame.	deg.
V_{cap}	Capacitor DC-link voltage.	V
α	Angle between d-axis stator current ($i_{d,s}$) and I_{max}.	deg.
p	Number of poles.	
$\overline{v}_{inv1}$	Voltage space vector of first inverter.	V
$\overline{v}_{inv2}$	Voltage space vector of second inverter.	V

Chapter 1

Background of Induction Motors Speed Control

Over the past few decades, field weakening operation of induction machines have been studied to expand the motor speed operation range without exceeding the available DC-link voltage. This thesis work studies the fielding weakening operation of open-ended winding induction motors where a new control strategy has been presented to enhance the motor operation range. This chapter first provides a brief, but explanatory review on induction motors and field-oriented control to set the foundation to understand the basic operation principle of induction motors and their well known vector control. Then, the voltage and current constraints of field-weakening operation, and different field-weakening operating regions are introduced to understand how motor torque, power, voltage, and current are behaving in the different field weakening regions.

1.1 Introduction

The induction motor is the most commonly used motor around the globe due to its high reliability, low cost, high starting torque, and wide speed operation range [1]. In industrial countries, induction motors consume approximately one-third of the energy generated [2]. Hence, control and performance optimization of induction motors received much interest and attention.

In order to understand the control of induction motors in the flux weakening region, the fundamental operation principle of this motor need to be introduced.

The simplest construction of the three phase squirrel-cage induction motor involves a stator that holds a three phase windings, 120 degree spatially phase shifted, a rotor, and an air gap with a constant thickness. The induction motor operation is based on the rotating magnetic field that is produced by the stator three windings when energized by an AC source. The rotating magnetic field has a constant angular speed and cuts through the rotor bars, inducing a rotor current as per Faraday's Law of electromagnetic induction. A current carrying conductor moving through a magnetic field will experience a mechanical force, which creates a torque that rotates the rotor of the motor.

The speed of the rotating magnetic field in rpm (revolutions per minute), also known as the synchronous speed (N_s), is defined as:

$$N_s = \frac{120\ f_s}{p} \tag{1.1}$$

This relationship is fundamental in the study of induction motors as it define the relation between the rotating magnetic field speed, the stator electrical supply frequency, f_s, and the number of poles, p.

The rotor accelerates up to a speed slightly lower than the stator magnetic field speed. If the rotor is rotating exactly at the synchronous speed (N_s), there will be no flux cutting at the rotor conductors, hence no induced $e.m.f.$ or current in the rotor winding. As a result, no torque will be produced. Due to this reason, induction motors rotate at a speed slightly lower than the stator magnetic field speed. The difference between the rotating magnetic field speed (ω_s)[1] and the rotor mechanical speed (ω_m) over ω_s is known as the slip, [3], and is given by:

$$slip = \frac{\omega_s - \omega_m}{\omega_s} \tag{1.2}$$

The value of this slip is one if the rotor is at standstill.

To control the speed and torque of these induction motors, different control schemes have been presented such as Volts/Hertz control [4], sensorless vector control, flux vector control, and field oriented control [5]. Field oriented control gives the best speed and

[1]Note that $\omega_s = 2\pi/60\ N_s$.

torque regulation among other control methods, which is the one adopted in this thesis work.

1.1.1 Field Oriented Control

Field-oriented control (FOC), also widely called vector control, was developed in the early of 1970s [6]. It is mainly based on the decoupling of the instantaneous stator current into flux producing current and torque producing current with the help of Park transformation (dq-frame).

The flux current is aligned with the d-axis and it does not change rapidly over time. This means that the flux current cannot be used for rapid motor performance control and it is better to keep it constant at rated value for maximum torque operation. This is preferred at low speed control. However, at high speed, flux weakening below the rated value is preferred to accelerate the motor beyond the rated base speed. On the other hand, the q-axis current can be changed rapidly so it is used to control the motor torque. This is why the q-axis current is referred to as the torque current.

With the knowledge of the required flux and torque currents, the slip frequency and the electrical motor frequency can be calculated using the following [7]: [2]

$$\omega_{sl} = \frac{R_r}{L_r}\frac{i_{qs}}{i_{ds}} \tag{1.3}$$

$$\omega_e = \omega_r + \omega_{sl} \tag{1.4}$$

The FOC is applied in d-q frame, which is rotating at the synchronous speed. For speed control purpose in d-q frame, the rotor speed (ω_r) is measured and added to calculated slip speed (ω_{sl}) to give the required d-q frame speed (ω_e).

The stator d&q voltages that drive the flux and torque currents can be calculated using the following [8]: [3]

[2] The subscript s means that all these quantities are referred to the stator side of the machine.

[3] All values (voltages and currents) in this thesis work are represented in peak values not RMS. This is because referring to peak values is common in control schemes as for example V_{ds} or V_{qs} in dq-frame are peak values. Furthermore, the voltage and current values are peak phase values, not line values.

$$v_{qs} = R_s i_{qs} + \omega_e L_s i_{ds} \tag{1.5}$$

$$v_{ds} = R_s i_{ds} - \omega_e (L_s - \frac{L_m^2}{L_r}) i_{qs} \tag{1.6}$$

The maximum fundamental phase voltage, active and reactive power can now be found by:

$$V_{max} = \sqrt{V_{qs}^2 + V_{ds}^2} \tag{1.7}$$

$$P = \frac{3}{2}(v_{qs} i_{qs} + v_{ds} i_{ds}) \tag{1.8}$$

$$Q = \frac{3}{2}(v_{qs} i_{ds} - v_{ds} i_{qs}) \tag{1.9}$$

1.2 Field Weakening Operation of Motor Drives

High speed capability of machines is required for applications, such as spindle, servo, traction, and electric vehicles (EVs) or hybrid electric vehicle drives [9]-[13]. Such applications can be achieved easily over an extended high speed range by means of field weakening operation of induction machines (IMs).

The field weakening (FW), also sometimes referred to as flux weakening, operation describes the strategy by which the motor's speed can be increased above it's rated base speed at the expense of reducing torque. FW operation is used for motor applications where achieving higher rotor speeds is desirable and producing lower torque is acceptable.

Field weakening enables higher speeds above base speed by reducing the motor back electromotive force (EMF)[4]. This back EMF is a voltage created when a coil, such as rotor coils, turns within a magnetic field and opposes the current driving voltage (supply

[4]Note that there are two different speeds: the rated speed and the base speed. The rated speed is the speed that is often given on the motor nameplate. The base speed is the speed after which the FW starts.

voltage). This back EMF voltage is a function of rotor speed and air gap flux (field). For a constant air-gap flux, as the rotor speed increases, the back EMF voltage is increasing. Hence, to drive motor current, the supply (driving) voltage increases as the rotor speed is increasing. However, this supply voltage has a limit defined by the DC-link voltage and pulse-width modulation strategy used. Once the supply voltage reaches a limit, the flux is weakened to reduce back EMF voltage, which as a result enables higher motor speeds.

FW is good for applications where higher speed is desirable, but increasing supply voltage is not acceptable, such as EVs. In EVs, the supply voltage is limited by the battery size. FW enables EVs to achieve higher speeds without the need for a higher battery voltage.

The main performance limiting factors in FW are the voltage and current ratings of both inverter and motor. This implies that to fully exploit the motor-drive capability, a control strategy must be adopted to maximize the motor output power and torque under the current and voltage constraints [10], [11], [14], [15].

1.2.1 Voltage and Current Constraints

The maximum phase voltage supplied by a pulse-width modulation (PWM) inverter is decided by the DC-link voltage and the PWM method used [15]. If pulse-width modulation with third-harmonic injection is used, the maximum (peak) fundamental phase voltage is given by:

$$V_{max} = \frac{V_{dc}}{\sqrt{3}} \tag{1.10}$$

Once the maximum phase voltage, V_{max}, is decided, the magnitude of the inverter voltage vector ($|\overline{v}|$) should be less than or equal to the maximum voltage, i.e. (1.11), regardless of the implemented reference frame.

$$|\overline{v}| \leq V_{max} \tag{1.11}$$

Moreover, the maximum current supplied to IM is usually limited by the inverter and the motor itself. Once the maximum current, I_{max}, is decided, the magnitude of the stator

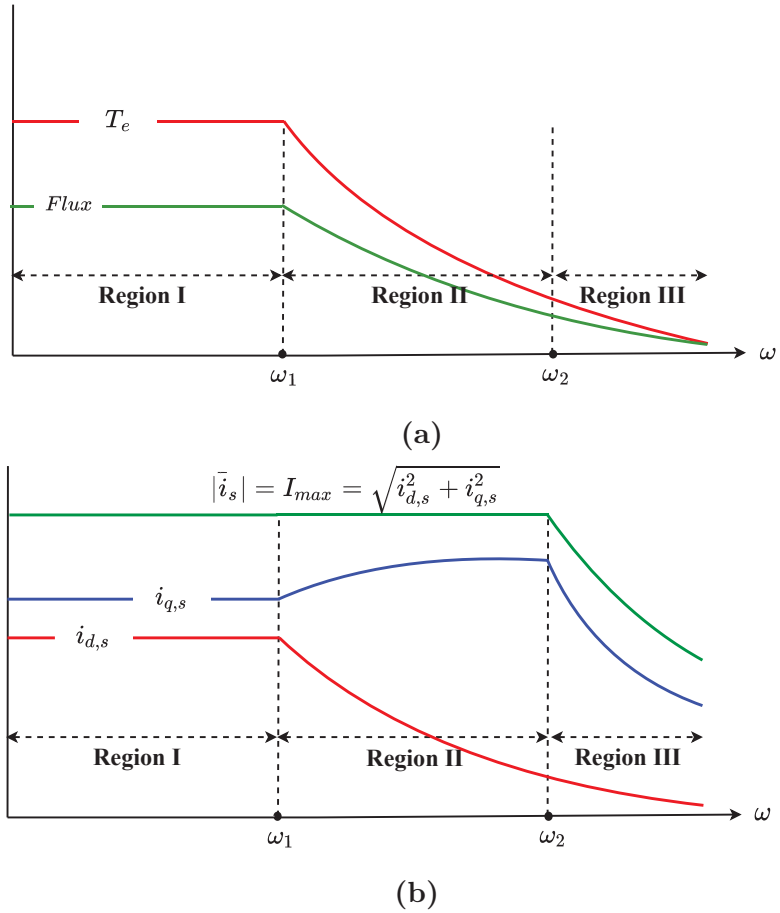

Figure 1.1: Operation speed zones: (a) Torque and motor flux versus speed characteristics, and (b) $i_{d,s}$, $i_{q,s}$ and $|\bar{i}_s|$ versus speed characteristics.

current vector ($|\bar{i}_s|$) should be less than or equal to the maximum current, i.e. (1.12), regardless of the implemented reference frame.

$$|\bar{i}_s| \leq I_{max} \tag{1.12}$$

1.2.2 Operating Regions

The operating range of the induction motor with the FW strategy can be divided into three regions as shown in Fig.1.1.[5]

[5] ω in this figure is the electrical supply frequency in rad/s, which is given by $\omega = 2\pi f$. At high speeds, the slip is negligible, i.e., $\omega \cong \omega_r$, where ω_r is the electrical rotor speed in rad/s.

Constant Torque Region [Region I] ($\omega < \omega_1$)

The flux current ($i_{d,s}$) is kept constant in this region as the drive can supply the motor with a voltage that keep the machine flux constant. Then, to have maximum current for maximum torque operation, the torque current ($i_{q,s}$) is held constant at rated value in this region as shown in Fig.1.1a & Fig.1.1b. Since the torque current is kept constant at the rated value in this region, it is called the constant torque region[6].

The output mechanical power is increasing in this region because the torque is held constant at the rated value and the speed is increasing, $P_{mech} = T_e \times \omega_m$.[7] This region extends to ω_1, which represents Region I speed limit.

This behaviour up to ω_1 can be obtained using the field-oriented control method. After ω_1, the applied stator voltage reaches a maximum limit define by the DC-link and the applied modulation strategy. Hence, the rotor speed cannot rise more using only the FOC and the FW operation needs to take place.

Field Weakening Region [Region II] ($\omega_1 < \omega < \omega_2$)

To increase the motor rotor speed above ω_1, the FW strategy is applied. According to the ($\frac{V}{Hz}$) ac motor operation principle, the motor flux is given by $\varphi = \frac{V}{\omega}$. In Region I, the flux is kept constant. Hence, fundamental voltage supplied to the motor increases as the rotor speed is increasing. However, the supplied fundamental voltage reaches a limit defined by the VSC DC-link voltage and PWM strategy used. The speed at which the voltage reaches the limit is referred to as ω_1. In Region II, the voltage cannot be increased so the flux is weakened while the speed is increasing, which is why this method is called flux weakening or field weakening. So in this region, the flux current ($i_{d,s}$), hence motor flux, is decreasing and $i_{q,s}$ is increasing to maintain the maximum phase current, see Fig.1.1. The output mechanical power is held constant in this region if real power supplied to the motor is maintained constant[8]. The torque is decreasing as the speed in increasing with

[6]Note that the waveforms shown in Fig.1.1 are the maximum values that you can get from a drive. This is why for example the torque current (torque) is held constant in the first region (because that is the maximum value you can get from a drive). For a usual drive operation, the torque is kept constant at the rated value during the acceleration period only, for having a fast acceleration performance. However, once the reference speed is approached, the torque is reduced to the value of the load applied to the drive.

[7]ω_m is the mechanical rotor speed in rad/s. This speed is given by $\omega_m = \frac{2}{P}\omega_r$.

[8]More details will be presented in Chapter 2, section 3.

the FW operation, Fig.1.1a. This region expands to ω_2, which represents Region II speed limit.

Decreasing Power Region [Region III] ($\omega > \omega_2$)

Once ω_2 is reached, the drive transfers to Region III. The overall machine phase current is decreasing in this region. As a result of that, the output mechanical power is decreasing as the speed is increasing in this region.

1.3 Thesis Statement

A FW controller is presented that extends the speed range in the field weakening region, output power and torque of a dual inverter drive using a floating capacitor bridge. This controller is also compared with other four FW control schemes, three of which are dual inverter drive (DID) schemes, in terms of performance, maximum stator voltage, speed extension ratio, speed acceleration time, available output power and torque. The presented scheme main features are as follows:

1. At low speeds, the main bridge connected to the main power supply is operated at Unity Power Factor (UPF). At high speeds and after the floating bridge connected to a floating capacitor reaches a maximum limit, the main bridge is operated at non-UPF to supply some reactive demand.
2. The presented scheme retains the same features of the UPF DID until a specific operating point and extends the drive output power, torque, speed acceleration performance, and per-unit speed over the UPF DID after that point.
3. The speed extension ratio is 9.2 times the base speed compared to 4, 5, 8.4 and 10.3 for a single inverter drive, UPF DID, single DC-link DID, and two isolated DC-links DID, respectively.
4. The presented scheme at a specific point has the same output power as the single DC-link DID and extends both the drive output power and per-unit speed after that point.

5. The maximum fundamental stator voltage is 0.83 p.u, 0.52 p.u, and 0.17 p.u higher compared to the single inverter drive, UPF DID, and single DC-link DID, respectively, and only 0.17 p.u lower than that of two isolated DC-links DID.

6. The capacitor voltage is kept decoupled from motor transient and transition from one FW operating region to another.

A control scheme that makes the floating bridge DC-link voltage variable and optimized to improve the overall drive efficiency both in low and high torque values is described as the future work.

The structure of the thesis report is as follows: Chapter 2 provides a brief explanatory review on different existing DID topologies and their FW operation to introduces the other FW control schemes that has been done in literature and their results. The voltage boundary limits in SCRF of five drives, four of which are DIDs, are described in Chapter 3, establishing the base for understanding how each drive behaves at low and high speed regions. Then, the presented work control scheme is described in Chapter 4, followed by its simulation and experimental results in Chapter 5. A comparison of the presented FW controller results with the other existing control schemes is also presented in Chapter 5. The floating bridge capacitor voltage is made variable to improve the DID efficiency in Chapter 5 and presented as a future work. The report is concluded in Chapter 6 by summarizing the key points of the work performed.

Chapter 2

Field Weakening Operation of Induction Motor Dual Inverter Drives

A brief explanatory review on different existing DID topologies and their FW operation is provided, which introduces the other FW control schemes that has been presented in literature and their results. Furthermore, different MB to FB DC-link voltage ratios are discussed to justify why a MB: FB ratio of (1:1) has been selected for the presented work. Then, the theoretical relationships that can be used to estimate the speed limit of the operating regions (Region I and Region II) are introduced. These relationships are used to calculate Region I speed limit and Region II speed limit theoretically. These relationships also clarify the parameters that affect these speed limits. Moreover, the ability to control the MB to operate at UPF or non-UPF requires the ability to control the active and reactive power supplied to the motor. This is achieved by using stator current reference frame, which is also described in this chapter.

2.1 Background

High speed machines are required for applications, such as, spindle, servo, and electric vehicles or hybrid electric vehicles [9] - [13]. The IM is the considered choice due to its high reliability, high starting torque, and wide speed operation range that can be achieved easily by means of a FW control scheme.

It is always desirable to retain the maximum output torque and power capability of a machine during the whole high speed operation range. Several control strategies have been reported in literature that differ in terms of performance, complexity of implementation, number of regulators, main control variables, and basis of flux level adjusting. A comparison between different IM field weakening methods showed that the voltage closed loop field weakening method outputs the maximum torque with a small computation burden [9]. The flux current gets modified with this method based on the voltage requested by the IM. This flux level adjusting method is based mainly on the method proposed by [10], which has been regarded as a useful method due to ease of implementation and low sensitivity to machine parameters [16]. It is also suitable for field weakening operation of DIDs using an open-ended winding induction machine (OEWIM).

The Dual Inverter Drive (DID) using an OEWIM reported in [17] has been regarded as a suitable topology for high speed applications [13]. The open-ended configuration was originally proposed to reduce the current ripple and boost voltage of permanent magnet synchronous machines [17]-[20]. Later on, it was also considered for induction machines.

OEWIM means that both machine stator winding ends are accessible and requires two inverters, one on each end. If both OEWIM ends are used and two inverter are connected, one on each end, the drive is called a DID. If only one end is used to connect a single inverter and the other end is shorted (Y-connection), the drive is called a single inverter drive. The DID using an OEWIM is used to boost the motor voltage compared to a single inverter drive. This voltage boost can be used to extend the motor speed range over the single inverter drive.

The two inverters for DID can be connected to a single DC power supply [21]-[27], to two separate DC power supplies [28], [29], or to a DC power supply and a floating capacitor bridge [12], [13], [30]-[33], as shown in Fig.2.1. Some of the main advantages this topology has over the traditional single inverter is its multilevel voltage, its high reliability, and its voltage boost [34], which can be used to extend both the constant torque region [13] and the field weakening region [30], [31]. This drive configuration also has several advantages over other multilevel converters with the same number of output levels, such as the NPC, where there is no neutral point voltage fluctuations, a lower DC-link voltage requirement, a greater number of available switching states for more flexible PWM schemes [32], and a lower component count [35].

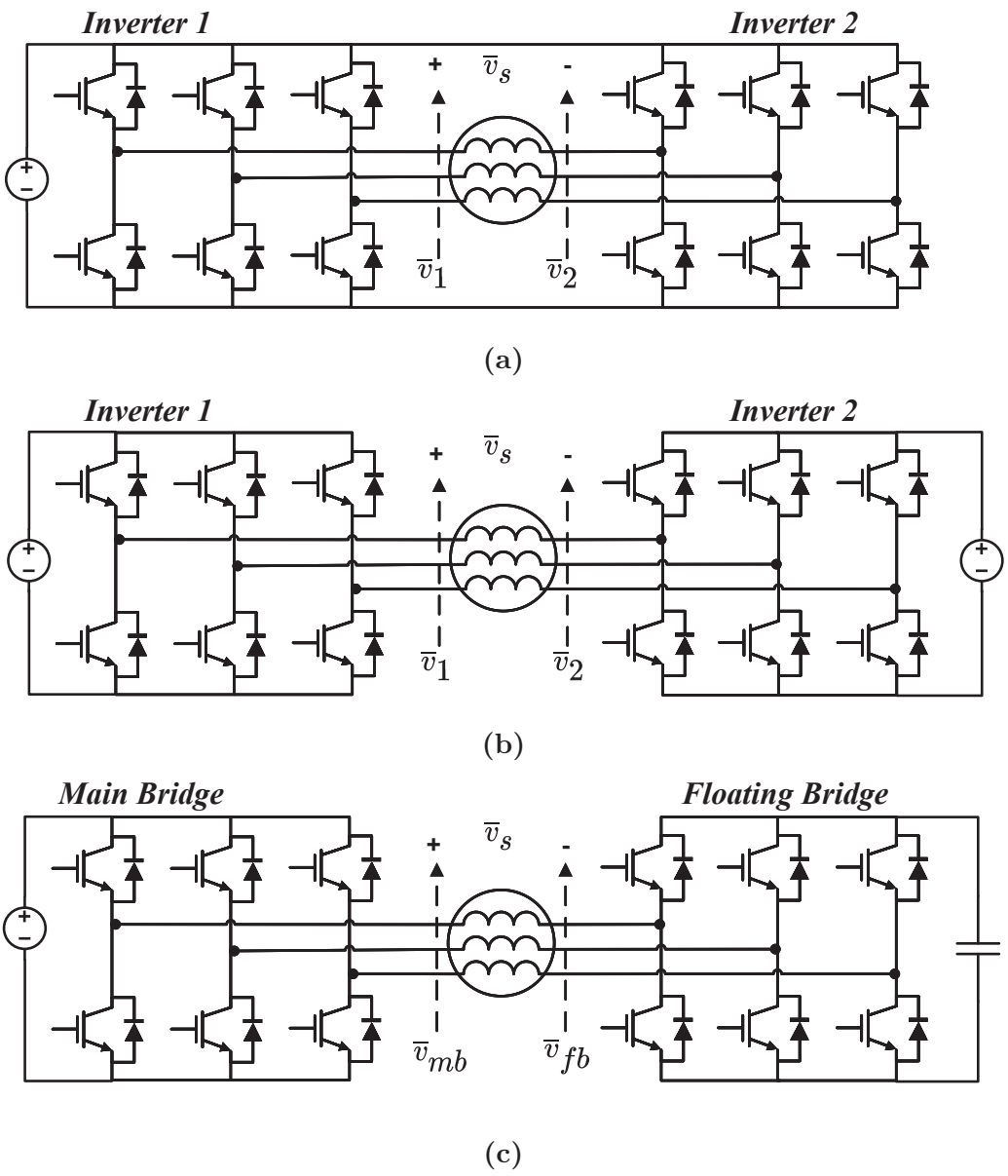

Figure 2.1: Dual inverter drive for open-end winding machines: (a) Single DC power supply, (b) two separate DC power supplies, and (c) single DC power supply with a floating capacitor bridge.

A DID using a single DC supply suffers from common-mode currents that circulate within the system. These zero sequence currents can be suppressed either by adding extra hardware, such as common mode chokes [17] and auxiliary switches [36], or additional level in the PWM control scheme [21]-[26]. These PWM schemes that eliminate common-mode

currents lower the PWM quality and the drive's voltage boost capability. When two isolated DC sources are used, Fig.2.1b, zero sequence currents are inherently eliminated and the drive's reliability is increased. However, two isolated DC sources further increase the cost, size, and weight of the drive.

The floating bridge DID, Fig.2.1c, has recently gained popularity in multilevel converter applications as it eliminates the common-mode current pathways without the need for a bulky common-mode reactor and reduces the drive size, weight, and cost [37].

The floating bridge (FB) capacitor is charged through the IM and its voltage can be regulated using a simple PI controller [13], [30], [31]. The motor reactive power requirement (VArs) can be supplied by the FB, while the main bridge (MB) can be operated at unity power factor (UPF) to maximize the output mechanical power [30], [31]. This boosts the motor phase voltage over what could be supplied using a single inverter drive. Hence, both the drive output capability and high speed range can be extended when compared to the single inverter drive.

The MB to FB DC-link voltage ratio (MB:FB DC-link voltage ratio) design is crucial in defining both the DC-link supply utilization and output PWM quality. Several ratios have been previously presented and discussed to enhance the inverter performance. A comparative study considering different possible voltage ratios (1:0.33, 1:0.5, 1:1, and 1:2) and a ratio selection strategy to boost the voltage utilization without degrading the PWM quality have been presented by [23]. Increasing the FB DC-link voltage to double the MB DC-link voltage for a MB:FB ratio of (1:2) has a diminishing return in terms of speed range extension, increases the voltage rating of the second inverter switches, and complicates the design process. A MB:FB ratio of 1:0.5 is usually used to improve the quality of the PWM voltage, which as a result reduces the current ripples. A 1:1 ratio is preferred as just one design is needed for both inverters and it gives a sufficient fundamental voltage boost, speed extension ratio, output mechanical power and torque. Hence, the FB DC-link voltage in this paper is made to be the same as the MB connected to the power source.

With the continuous development of power electronic converters, power electronic devices and materials, electric motor driven solutions are increasing in speed and power, especially in industrial applications such as spindles, pumps, and compressors, with an IM speed range from 10k – 100k RPM, [38], [39]. A summary of the key industrial high speed

machine applications and their corresponding speed is presented in [38]. With such a high speed demand in the market, it is necessary to reach high per unit speeds. The presented work for example can boost the speed up to 9 p.u. without adding extra hardware components to the system when compared to MB-UPF DID that always operates the MB at UPF and achieves a 5 p.u. speed. This adds an additional attractive feature to the presented work. Furthermore, the major development in the area of high speed machine materials and components, including soft and hard magnetic materials, stator and rotor lamination materials, rotor-bar and end-ring materials, has improved the operating physical machine boundaries, allowing for ultra-high speeds with high power densities [38], [39]. A study of the recent technologies used in high speed machines, developments in high speed machine materials and components and their operating physical boundaries, and key applications of high speed machines is presented in [38]. It has been shown that the highest speed can be achieved through solid-rotor IM technology.

The DID control strategy with a FB for high-speed operation of induction motors has been first presented by [30] to compensate for the reactive voltage demand at high speeds. It was found that if the reactive voltage is supplied only by the FB, Region II can be extended to 4.5 times the base speed. Later in [31], a robust control scheme with a capacitor voltage balancing is presented. It has been shown that both the drive output power capability and the field weakening speed range can be extended by operating the MB at UPF and depending only on the FB to supply the motor reactive demand. However, this control scheme, also reported in [33], [40], uses an extra PI controller to maintain UPF operation of the MB, which increases the scheme complexity. The efficiency of this UPF DID has been improved at low and high speed regions by making the FB DC-link voltage variable with the operating conditions [33]. The efficiency improvement is visible more around the base speed and at high load. At low loads around the base speed, the reactive demand of the motor is high, which results in higher capacitor voltage and lower drive efficiency.

The FB capacitor voltage is decoupled from the motor transients in [13] by introducing a second reference frame named the stator current reference frame (SCRF). This reference frame along with the rotor flux reference frame (RFRF) will be used to describe a field weakening controller for DID using a FB. The RFRF is used to decouple the stator current into torque and field components, whereas the SCRF is used to decouple the motor demand into active and reactive components, which simplifies the control scheme and adds more flexibility. The SCRF also allows the MB to supply some reactive demand, which in turn

adds additional voltage boost that can be used in the high speed region. When operating at less than base speed, this voltage boost can be used to lower the DC supply voltage [13], which also lowers the device voltage stresses and power losses.

2.2 Mathematical Model

According to the voltage constraints[1], the magnitude of the bridge voltage vector ($|\overline{v}|$) should be less than or equal to the maximum voltage (V_{max}). For the floating capacitor drive configuration, this means that the magnitude of the MB voltage vector ($|\overline{v}_{mb}|$) and the FB voltage vector ($|\overline{v}_{fb}|$) should be less than or equal to the maximum voltage, i.e. (2.1). This is assuming that the MB to FB DC-link voltage ratio is 1:1, which means $V_{max,mb} = V_{max,fb} = V_{max}$. This DC-link voltage ratio is desirable since just one converter design is needed and the voltage stress is similar for both converters.

$$\begin{aligned} |\overline{v}_{mb}| &\leq V_{max} \\ |\overline{v}_{fb}| &\leq V_{max} \end{aligned} \tag{2.1}$$

2.2.1 Equations of Induction Machine

The induction machine equations are described by [8]:

$$\overline{v}_s = R_s\bar{i}_s + j\omega\overline{\varphi}_s + \frac{d\overline{\varphi}_s}{dt} \tag{2.2}$$

$$0 = R_r\bar{i}_r + j(\omega - \omega_r)\overline{\varphi}_r + \frac{d\overline{\varphi}_r}{dt} \tag{2.3}$$

$$T = \frac{3}{2}p(\frac{L_m}{L_r}\varphi_r)i_{qs} \tag{2.4}$$

In the rotor-flux-oriented reference frame, the rotor flux depends only on i_{ds} as (2.5) implies.

[1] See sub-section 1.2.1 for voltage constraints detail.

$$\varphi_r = L_m i_{ds} \tag{2.5}$$

Substituting by the rotor flux (2.5), in (2.4) leads to the following expression of the motor torque:

$$T = \frac{3}{2} P \frac{L_m^2}{L_r} i_{ds} i_{qs} \tag{2.6}$$

(2.6) shows that the torque is proportional to the product of currents i_{ds} and i_{qs}. If motor flux current (i_{ds}) is maintained constant, the motor torque will depend only on the torque current (i_{qs}).[2]

At steady state, (2.2) and (2.3) are described by:

$$\overline{v}_s = R_s \overline{i}_s + j\omega \overline{\varphi}_s \tag{2.7}$$

$$0 = R_r \overline{i}_r + j(\omega - \omega_r) \overline{\varphi}_r \tag{2.8}$$

If the resistance voltage drop is neglected at high speeds, (2.7) and (2.8) are reduced to

$$\overline{v}_s \cong j\omega \overline{\varphi}_s \tag{2.9}$$

$$0 \cong j(\omega - \omega_r) \overline{\varphi}_r \tag{2.10}$$

(2.9) implies that the voltage of the stator is strongly affected by the stator back electromotive force (EMF). This means that as the speed is increasing, the EMF voltage will increase, which as a result increases the stator voltage (v_s). (2.10) implies that at high speeds, the slip is negligible, i.e., $\omega \cong \omega_r$.

[2]The i_{ds} current is usually called the flux current, whereas the i_{qs} current is usually called the torque current. This definition will be used through the thesis.

2.2.2 Floating Capacitor Bridge Equations

The stator voltage vector of a DID using a floating capacitor bridge is given by (2.11), where $\overline{v}_{mb}$ and $\overline{v}_{fb}$ are the output voltage vectors of the MB and FB, respectively.

$$\overline{v}_s = \overline{v}_{mb} - \overline{v}_{fb} \tag{2.11}$$

The MB can supply both real and reactive power. Hence, $\overline{v}_{mb}$ can have both a real component in phase with the motor current and a reactive component 90° out of phase with respect to the motor current. The FB is connected to a capacitor, so the FB is only capable of supplying reactive power. Therefore, $\overline{v}_{fb}$ is usually 90° out of phase with respect to the motor current.

$\overline{v}_{mb}$ and $\overline{v}_{fb}$ are equal to:

$$\overline{v}_{mb} = (v_{P,mb} + jv_{Q,mb})\frac{\overline{i}_s}{|\overline{i}_s|} \tag{2.12}$$

$$\overline{v}_{fb} = (v_{P,fb} - jv_{Q,fb})\frac{\overline{i}_s}{|\overline{i}_s|} \tag{2.13}$$

Neglecting the parasitic losses in the FB, at steady state, the DC-link voltage of the FB should be held constant. Consequently, the active voltage component absorbed by the FB to maintain the capacitor charged will be zero ($v_{P,fb} = 0$) and (2.13) becomes:

$$\overline{v}_{fb} = (-jv_{Q,fb})\frac{\overline{i}_s}{|\overline{i}_s|} \tag{2.14}$$

2.3 Decoupling into Active and Reactive Components

There are two reference frames that has been used in this work. The first one it is called the Rotor Flux Reference Frame (RFRF). This reference frame is used to decouple the machine current into flux current ($i_{d,s}$) and torque current ($i_{q,s}$), Fig.2.2. The flux current controls the machine flux, whereas the torque current controls the machine torque. The angle between the machine current ($\overline{i}_s$) and $i_{d,s}$ is α, which is given by (2.15).

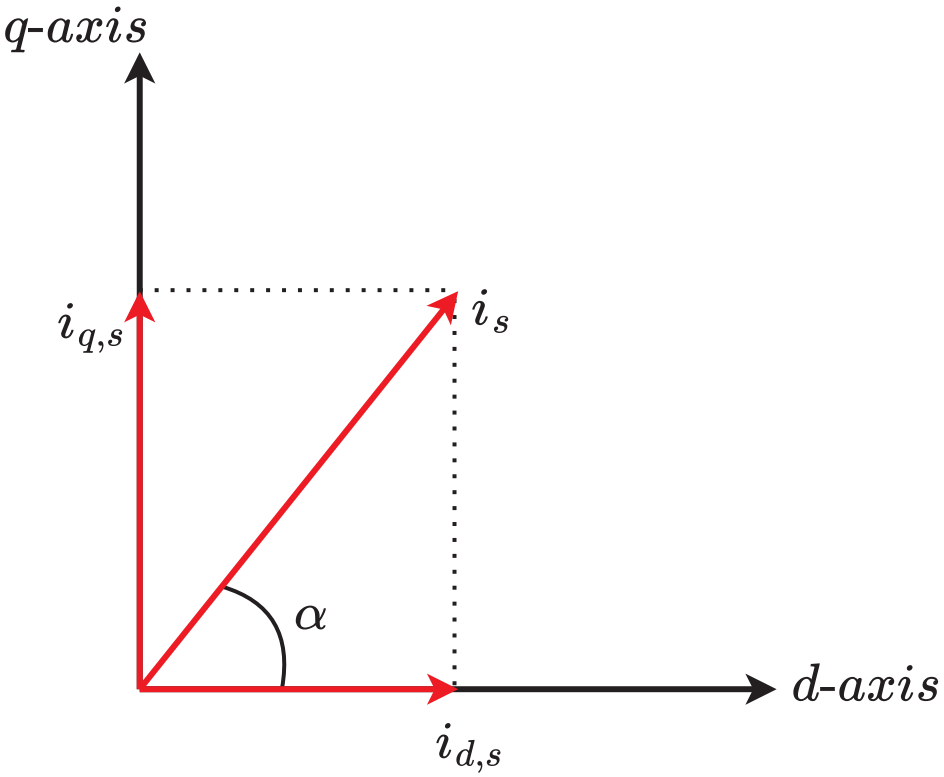

Figure 2.2: Decoupling the stator voltage into active and reactive components using the stator current reference frame.

$$\alpha = \tan^{-1}(\frac{i_{q,s}}{i_{d,s}}) \tag{2.15}$$

It is clear that the objective of controlling the MB to supply some reactive power after the FB reaches a maximum limit requires the ability to control the active and reactive power of both the MB and FB. To achieve this, the power required by the motor need to be decoupled into active and reactive components. The RFRF only decouples the stator current into flux and torque components. The Stator Current Reference Frame (SCRF) can be used to achieve this purpose as the motor voltage can be decoupled into active and reactive components. Any voltage component aligned (in phase) with the stator current will be an active voltage component (V_P) and will cause a real power flow, see Fig.2.3. Any voltage component 90° out of phase with the stator current will be a reactive voltage component (V_Q) and will cause a reactive power flow. Hence, the stator current vector

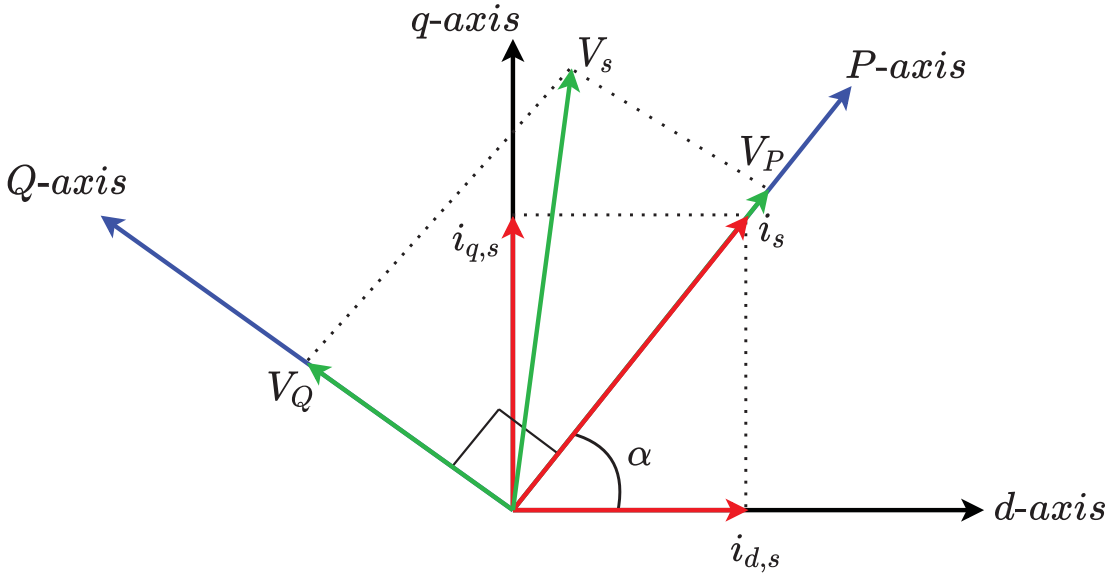

Figure 2.3: Decoupling the stator voltage into active and reactive components using the stator current reference frame.

will be regarded as the real power axis (P-axis), whereas the reactive power axis (Q-axis) will be leading the $\bar{i}_s$ by 90°, Fig.2.3. The P-axis of the SCRF is leading the RFRF d-axis by an angle α. Hence, the phase of the SCRF is given by:

$$\theta_{current} = \alpha + \theta_{flux} \tag{2.16}$$

Taking the P-axis to be aligned with the $\bar{i}_s$ means that the active current component ($i_{P,s}$) is equal to the magnitude of the stator current vector $|\bar{i}_s|$, whereas the reactive current component ($i_{Q,s}$) is equal to zero. Then according to this, the active power (P) and reactive power (Q) in SCRF are given by:

$$P = \frac{3}{2}(|\bar{i}_s| v_P) \tag{2.17}$$

$$Q = \frac{3}{2}(|\bar{i}_s| v_Q) \tag{2.18}$$

According to (2.17) and (2.18), for a constant machine current (i_s), the active power can be controlled by the active voltage component (V_P), whereas the reactive power can be controlled by the reactive voltage component (V_Q).

2.4 Speed Limits of Dual Inverter Drive Operating Regions

The goal of any field weakening strategy is to maximize the drive's mechanical output power, torque, and to extend the field weakening region as much as possible. If motor losses are ignored, the motor input active power will nearly be equal to the output mechanical power (P_{mech}) as given by (2.19). Hence, to boost P_{mech}, motor input active power supplied by the MB should be boosted.

$$P_{mb} \cong P_{mech} \tag{2.19}$$

For,

$$P_{mb} = \frac{3}{2}(|\bar{i}_s| v_{P,mb}) \tag{2.20}$$

Note that for a constant stator phase current, the active power is a direct function of the MB active voltage. Increasing the active voltage, will increase the active power supplied to the motor, which as a result increases the output mechanical power.

The reactive powers of MB, FB, and IM are given by:

$$Q_{mb} = \frac{3}{2}(|\bar{i}_s| v_{Q,mb}) \tag{2.21}$$

$$Q_{fb} = \frac{3}{2}(-|\bar{i}_s| v_{Q,fb}) \tag{2.22}$$

$$Q_s = \frac{3}{2}\omega L_s(i_{ds}^2 + \sigma i_{qs}^2) \tag{2.23}$$

Where, σ is the leakage coefficient, which is defined as $\sigma = 1 - \frac{L_m^2}{L_s L_r}$.

2.4.1 Constant Torque Region

In this region, the MB supplies no reactive demand, i.e. $Q_{mb} = 0$. This means that the full reactive power demand of IM is supplied by the FB. Then, equating (2.22) to (2.23) and solving for $v_{Q,fb}$, gives [31]:

$$v_{Q,fb} = \omega L_s \frac{i_{ds}^2 + \sigma i_{qs}^2}{\sqrt{i_{ds}^2 + i_{qs}^2}} \tag{2.24}$$

According to the voltage constraints,[3] the magnitude of the MB voltage vector ($|\overline{v}_{mb}|$) should be less than or equal to the maximum voltage, i.e. $|\overline{v}_{mb}| \leq V_{max,mb}$. Since in this region, the MB supplies no reactive demand, then the MB voltage constraint becomes:

$$v_{P,mb} \leq V_{max,mb} \tag{2.25}$$

Substituting (2.9), (2.11), (2.14), and (2.24) in (2.25) and simplifying, yields

$$\omega L_s \frac{(1-\sigma) I_{ds} I_{qs}}{|\bar{i}_s|} \leq V_{max,mb} \tag{2.26}$$

Since ideally at this region limit, the MB maximum capability is used to supply only active voltage demand, i.e. $v_{P,mb} = V_{max,mb}$, then Region I speed limit is defined by:

$$\omega_1 = \frac{V_{max,mb}\ I_{max}}{(1-\sigma) I_{ds} I_{qs} L_s} \tag{2.27}$$

For $I_{qs} = \sqrt{I_{max}^2 - I_{ds}^2}$, (2.27) becomes: [4]

[3] Voltage and current constraints are described in section 1.2.1.

[4] Notice that i_{ds} is substituted by the rated value I_{ds}. This is correct since ideally at this region limit, the FW hasn't started yet.

$$\omega_1 = \frac{V_{max,mb}\ I_{max}}{(1-\sigma)I_{ds}\sqrt{I_{max}^2 - I_{ds}^2}L_s} \tag{2.28}$$

This equation shows that the speed limit of Region I is only a function of the MB maximum voltage ($V_{max,mb}$). This is because the MB active voltage is the current driving voltage. Once the MB reaches its maximum voltage, the drive hits it's Region I limit and moves to Region II. The maximum phase current (I_{max}) is kept constant at the rated value for maximum torque operation, whereas the flux current is kept constant at rated value for constant torque operation in Region I.

The controller presented retains the same features of the UPF controller by operating the MB at UPF until the FB hits its maximum voltage [5]. Hence, it will have the same Region I speed limit equation as UPF FW controller reported in [31].

2.4.2 Field Weakening Region

In this region, the FB hits its maximum reactive power (also maximum reactive voltage limit). If UPF FW controller is used, the DID will hit its Region II limit when the FB hits its maximum reactive power limit. However, the presented FW controller can operate the MB to supply some of the reactive power demand, which as a result extends this region (Region II) over the UPF FW controller. The amount of reactive power supplied by the MB is the total stator reactive power demand minus the FB maximum supplied reactive power. Hence, the MB reactive power is given by:[6]

$$Q_{mb} = Q_s + Q_{fb} \tag{2.29}$$

The total reactive voltage supplied to the IM can be found by substituting (2.21), (2.22), and (2.23) into (2.29) and re-arranging

$$v_{Q,mb} + V_{max,fb} = v_{Q,s} = \frac{\omega L_s(i_{ds}^2 + \sigma i_{qs}^2)}{|\bar{i}_s|} \tag{2.30}$$

[5] More detail on presented FW controller operation principle is described in the next section.

[6] Note that Q_{fb} term has a negative sign (see (2.22)). After taking this negative sign to outside, (2.29) becomes $Q_{mb} = Q_s - Q_{fb}$.

(2.30) shows that the total reactive voltage supplied to the IM ($v_{Q,s}$) at high speeds is the maximum FB voltage plus the MB supplied reactive voltage. If the current components are rewritten in polar form:

$$i_{ds} = I_{max} \cos(\alpha) \tag{2.31}$$

$$i_{qs} = I_{max} \sin(\alpha) \tag{2.32}$$

And then combined with (2.30), the speed limit of the field weakening region (ω_2) can be found as:

$$\omega_2 = \frac{V_{Q,s}}{L_s I_{max}(\cos^2(\alpha) + \sigma \sin^2(\alpha))} \tag{2.33}$$

Assuming $\alpha = \pi/2$, gives:

$$\omega_2 = \frac{V_{Q,s}}{L_s I_{max} \sigma} \tag{2.34}$$

By assuming that $\alpha = \pi/2$ in (2.34), we assume that $i_{d,s} \cong 0$ and $i_{q,s} \cong I_{max}$ at Region II speed limit. The validation of this assumption is shown in Chapter 5. Note that $V_{Q,s}$ for the presented scheme is given by:

$$V_{Q,s} = v_{Q,mb} + V_{max,fb} \tag{2.35}$$

(2.34) shows that the speed of the field weakening region (Region II) is only a function of the reactive voltage supplied to the IM by both the MB and the FB. At the beginning of Region II, the reactive voltage is fully supplied by the FB and the MB is operated at UPF, i.e. $v_{Q,mb} = 0$.[7] After the FB hits its maximum voltage ($V_{max,fb}$), the MB is operated at non-UPF and supplies some reactive demand ($v_{Q,mb}$). The higher the reactive voltage supplied by the MB, the wider is the Region II. Once the MB cannot supply more reactive demand, Region II speed limit, ω_2, is reached.

[7] In other words, when Region II starts, the FB hasn't reached its maximum limit yet, so the MB is operated at UPF to boost the output mechanical power. This operation is maintained until the FB reaches its maximum limit.

The active voltage supplied to the stator ($v_{P,s}$) is given by:

$$\omega L_s \frac{(1-\sigma) i_{ds} i_{qs}}{|\vec{i}_s|} = v_{P,s} \tag{2.36}$$

Substituting for (2.34) in (2.36) and simplifying the equation gives:

$$\tan(\alpha) = (\frac{1}{\sigma} - 1) \frac{v_{Q,mb} + V_{max,fb}}{v_{P,s}} \tag{2.37}$$

Since $\tan(\alpha) = \frac{i_{qs}}{i_{ds}}$, then the torque current (i_{qs}) at Region II limit is given by:

$$i_{qs} = (\frac{1}{\sigma} - 1) \frac{v_{Q,s}}{v_{P,s}} i_{ds} \tag{2.38}$$

2.4.3 Decreasing Power Region

Once ω_2 is reached, the drive transfers to Region III. Since both the MB and FB cannot supply more reactive voltage, the presented controller decreases I_{max} of (2.34) to further increase the speed beyond ω_2 in Region III. This is achieved by decreasing $i_{q,s}$ as the speed is increasing in Region III, which results in decreasing the overall machine current. As a result, the output mechanical power is decreasing as the speed is increasing in this region.

2.5 Speed Limits of Single Inverter Drive Operating Regions

The operating regions of induction machines fed by a single inverter drive are well known in literature [10], [31], [41]. Region I and II speed limits are given by (2.39) and (2.40), respectively.

$$\omega_1 = \frac{V_{max}}{\sqrt{I_{ds}^2 (L_s^2 - (\sigma L_s)^2) + (\sigma L_s I_{max})^2}} \tag{2.39}$$

$$\omega_2 = \frac{\sqrt{1+\sigma^2}}{\sqrt{2}L_s}\frac{V_{max}}{\sigma I_{max}} \tag{2.40}$$

2.6 Summary

A brief review on FW operation of different existing DID topologies is provided. The floating capacitor bridge dual inverter drive can eliminate the circulating currents and reduce the drive's size and cost when compared to two isolated DC power supplies. The motor voltage can be decoupled into active and reactive components using the stator current reference frame. The active power (real power) is directly proportional to the active voltage for a constant motor current. The same relationship is applied to the reactive power as it is proportional to reactive voltage for a constant motor current.

The constant torque region speed limit is only a function of the main bridge maximum fundamental voltage. This is because the MB voltage is the active voltage, which is the current driving voltage. Once this voltage reaches the maximum limit, Region I speed limit is approached and the field is weakened after. The field weakening region speed limit is only a function of the reactive voltage supplied to the motor. Once the reactive voltage supplied to the motor reaches a limit, the drive hits its Region II speed limit.

Chapter 3

Voltage Boundary Limits of Dual Inverter Drives

The SCRF is used to decouple the motor voltage into active and reactive voltage components. For a constant motor phase current, increasing the active voltage will increase the active power, whereas increasing the reactive voltage will increase the reactive power. The maximum active and reactive voltages that can be supplied by the drive at different speeds represent the voltage boundary limit of that drive. The voltage boundary limits in SCRF for different motor drives are presented that can be used to understand how the motor voltage vector is behaving as the speed is increasing with each drive topology. Furthermore, the results of the presented FW controller can be predicted and compared to the other drive's FW controllers using these voltage boundary limits.

3.1 Main Bridge Unity Power Factor

In UPF DID, the main bridge connected to the main power source is always operated at UPF and the floating bridge connected to the floating capacitor is the only reactive power source. The output active (V_P) and reactive (V_Q) voltage limit of this drive is shown in Fig.3.1a. Curve segment AB gives the maximum output voltage of the single inverter drive. Operation point A corresponds to the drive supplying no reactive demand, which is not a feasible operating point. As the reactive demand of the motor increases, the operation point moves along curve segment AB, reducing V_P while increasing V_Q, see Fig.3.1a. ACB represents the voltage capability of a 1:1 FB-DID operating the MB at

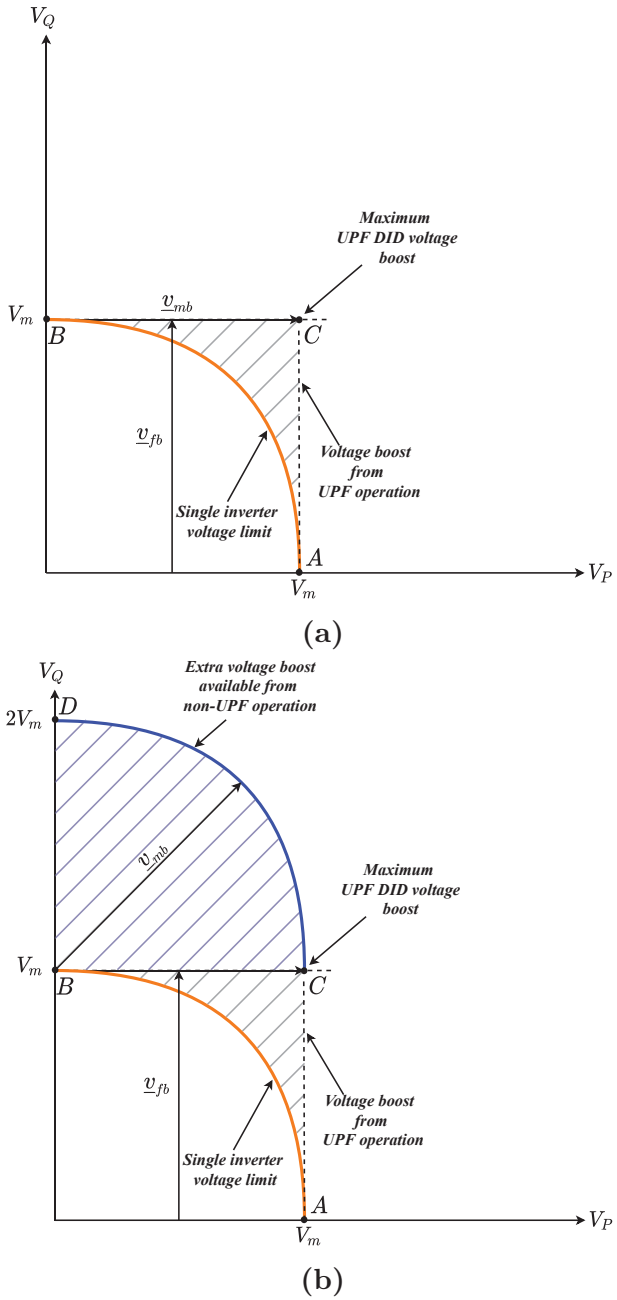

Figure 3.1: Drive's output active (V_P) and reactive (V_Q) voltage limits: (a) UPF FW controller, (b) presented FW controller.

UPF. Since the MB is only operated at UPF, it can supply only active power. This is why its voltage vector ($\overline{v}_{mb}$) is always horizontal across V_P-axis, Fig.3.1a. The FB is connected to a capacitor, so it can supply only reactive power. This is why its voltage vector ($\overline{v}_{fb}$)

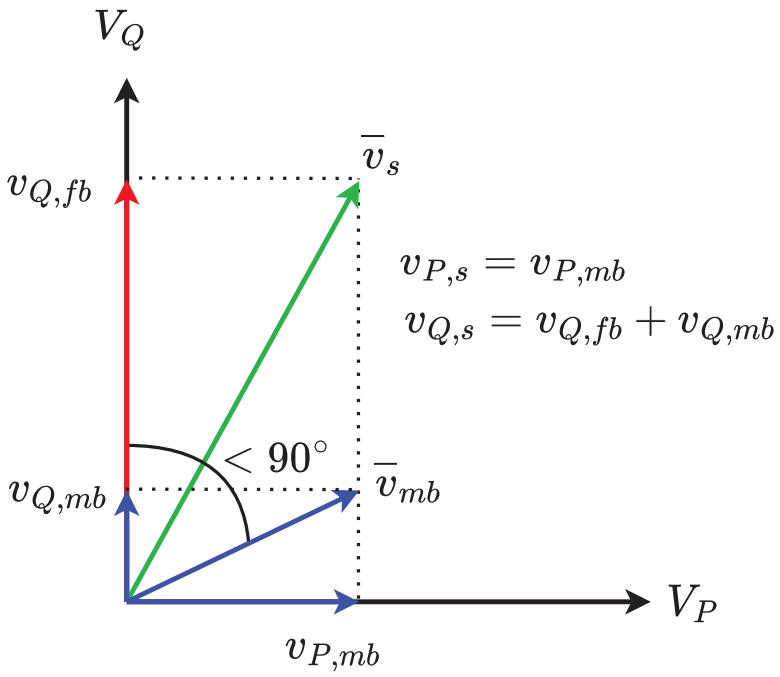

Figure 3.2: Voltage vectors of motor, MB, and FB.

is always vertical across V_Q-axis. As a result, that gives the square area represented by ACB as a voltage boundary limit for this drive.

As can be seen, when the MB voltage vector is always horizontal for UPF operation, both the MB and FB hits their maximum voltage at point C. The maximum voltage applied by both the MB and FB at point C is given by:

$$V_s = \sqrt{V_{P,s}^2 + V_{Q,s}^2} \tag{3.1}$$

Since the MB is the only source of active power (active voltage) and FB is the only source of reactive power (reactive voltage), then $V_{P,s} = V_{max,mb}$ and $V_{Q,s} = V_{max,fb}$. Moreover, for a 1:1 DID ratio, which is the ratio considered in this work, $V_{max,mb} = V_{max,fb} = V_{max}$, where V_{max} is the single inverter drive maximum voltage. Hence, ideally, the maximum fundamental voltage applied to the motor for a UPF DID is given by:

$$V_s = \sqrt{V_{max,mb}^2 + V_{max,fb}^2} = \sqrt{2}\, V_{max} \tag{3.2}$$

Fig.3.3a further demonstrates how the UPF DID behaves as the speed is increasing into the FW region. In Region I, the MB is operated at UPF and the FB supplies the reactive power demand. Once the MB reaches its maximum voltage limit, Region I speed limit (ω_1) is reached. The FB keep supplying the reactive power demand in Region II until it hits its maximum voltage limit. This limit corresponds to point C of Fig.3.1a and represents Region II limit. The maximum stator voltage at Region III is kept constant and the speed is increased further beyond (ω_2) by decreasing the motor phase current as the speed increases.[1]

3.2 Presented Work

The output active (V_P) and reactive (V_Q) voltage limit of the presented work is shown in Fig.3.1b, where ACD represents the maximum voltage capability of a 1:1 FB-DID operating the MB to supply some reactive demand. As can be seen, when the MB UPF constraint has been removed and the MB is controlled to supply some reactive demand, it results in the extra voltage boost portion BCD that can be used to supply more reactive requirement at high speeds. The maximum reactive voltage that can be supplied by this controller is $2V_m$, which is the same as the maximum reactive voltage supplied by a DID with two separate DC supplies. V_m is the single inverter drive maximum voltage.

In the presented DID FW control scheme, at low speeds, the MB is operated at UPF to boost the output mechanical power, whereas the FB is used to supply the motor reactive demand, until the FB reaches its maximum voltage. The main bridge is then used to supply some of the reactive demand, which in turn extends Region II, maximizes the output mechanical power and torque. This means that the presented work can maintain the UPF DID benefits until the FB reaches a limit and boosts the drive performance after.[2]

The vector addition of both the MB voltage vector ($\overline{v}_{mb}$) and the FB voltage vector ($\overline{v}_{fb}$) to give the overall machine voltage vector ($\overline{v}_s$) is further demonstrated in Fig.3.2. The

[1] More detailed description of Region III can be found in subsection 2.4.3.

[2] The FB voltage limit is represented by point C in Fig.3.1.

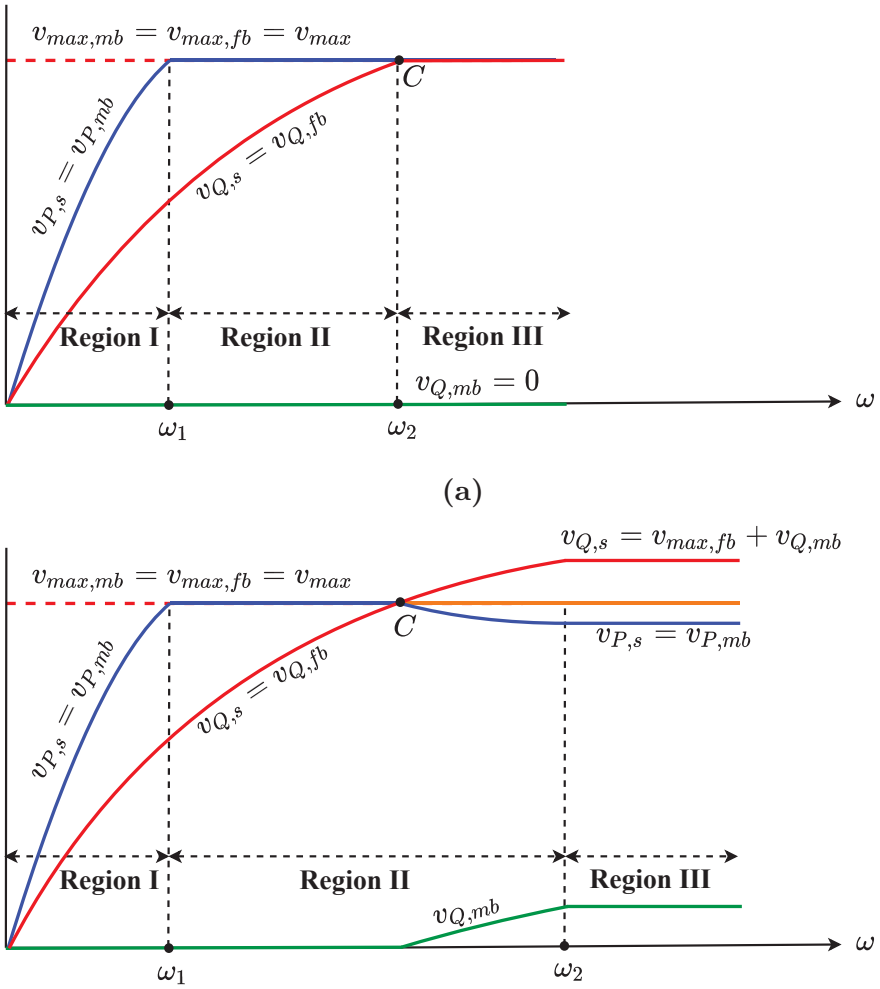

Figure 3.3: Drive's behavior in FW region: (a) UPF FW controller, (b) presented FW controller.

motor active demand is supplied only by the MB (3.3), whereas the motor reactive demand is supplied by both the MB and the FB (3.4)[3], see Fig.3.2.

$$v_{P,s} = v_{P,mb} \tag{3.3}$$

$$v_{Q,s} = v_{Q,fb} + v_{Q,mb} \tag{3.4}$$

[3]Note that the MB supplies reactive demand only when the FB reaches a maximum limit. Hence, $v_{Q,fb} = V_{max,fb}$ if $v_{P,fb}$ is ignored.

The operation of the presented control scheme as the speed increases into the FW region is further demonstrated in Fig.3.3b. The presented work maintains the same performance of UPF DID until point C, which represents the point where the FB reaches its maximum voltage limit. Hence, both DIDs have the same Region I speed limit (ω_1). After point C, the MB voltage vector is moving along curve segment CD reducing V_P and increasing V_Q, see Fig.3.1b and Fig.3.3b. The total reactive voltage supplied to the motor after point C is given by $v_{Q,s} = V_{max,fb} + v_{Q,mb}$. When comparing Fig.3.3a and Fig.3.3b, for the UPF DID and the presented work, respectively, we can see that Region II range has been greatly extended. [4]

3.3 Single DC Power Supply

A DID using a single DC supply can experience common-mode (zero-sequence) circulating currents. These currents can be suppressed to varying degrees of success by active circulating current suppression using PWM control [21]-[25]. The maximum voltage of this DID is reduced by 15% compared to that of two separate DC-links DID if a circulating current elimination method has been implemented [21]. This means that the maximum fundamental voltage of the single DC power supply DID is reduced from $2V_m$ to $1.7V_m$. Hence, the single DC-link DID maximum voltage capability is defined by curve segment EF, see Fig.3.4a. It is worth noting that point H in Fig.3.4a is where the single DC-link DID starts to behave the same as the presented scheme. This means that exactly at point H, both presented and single DC-link DIDs will have the same (V_P) and (V_Q). After which, the presented scheme has an advantage over the single DC-link DID.

3.4 Two Isolated DC Power Supplies

Zero sequence currents are inherently eliminated when two isolated DC supplies are used. The maximum voltage limit of this DID is defined by curve DG, Fig.3.4b. However, the

[4] Although the MB after point C is operated at non-UPF, the drive output mechanical power is still higher than UPF DID, which is explained in sub-section 5.2.2.

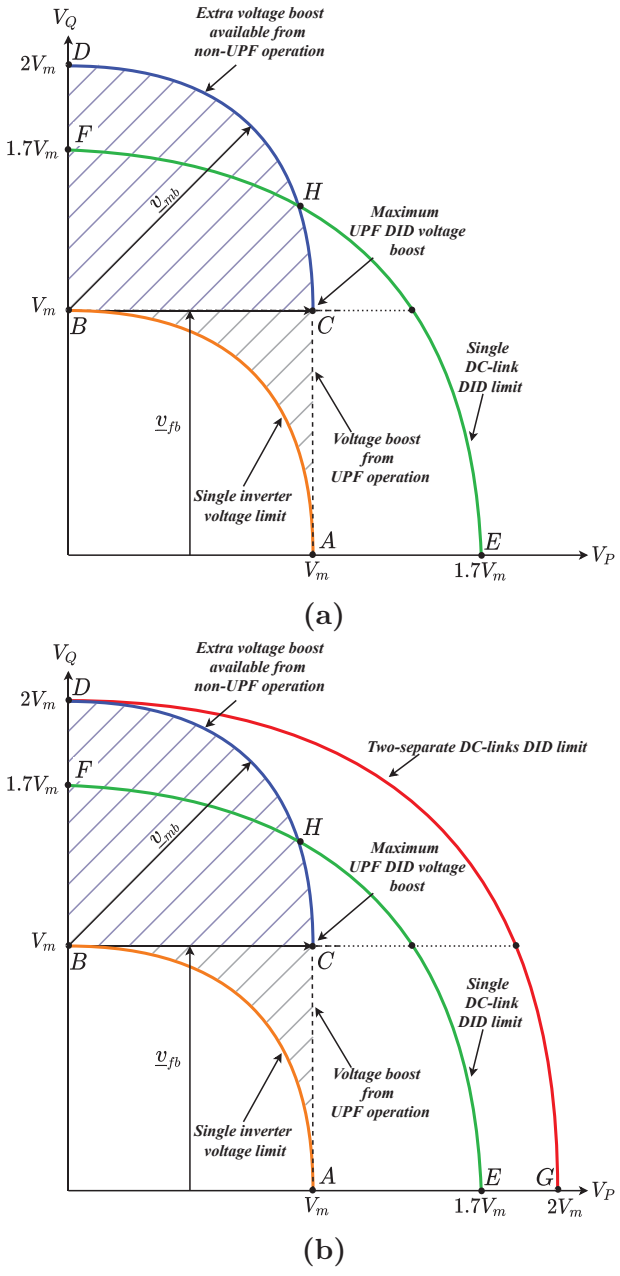

Figure 3.4: Drive's output active (V_P) and reactive (V_Q) voltage limits: (a) Single DC-link FW controller, (b) two separate DC-links FW controller.

use of two separate DC-links increases the complexity, cost, size, and weight of the drive system.

In order to analyze the system performance, two rules can be defined based on the derived system equations.

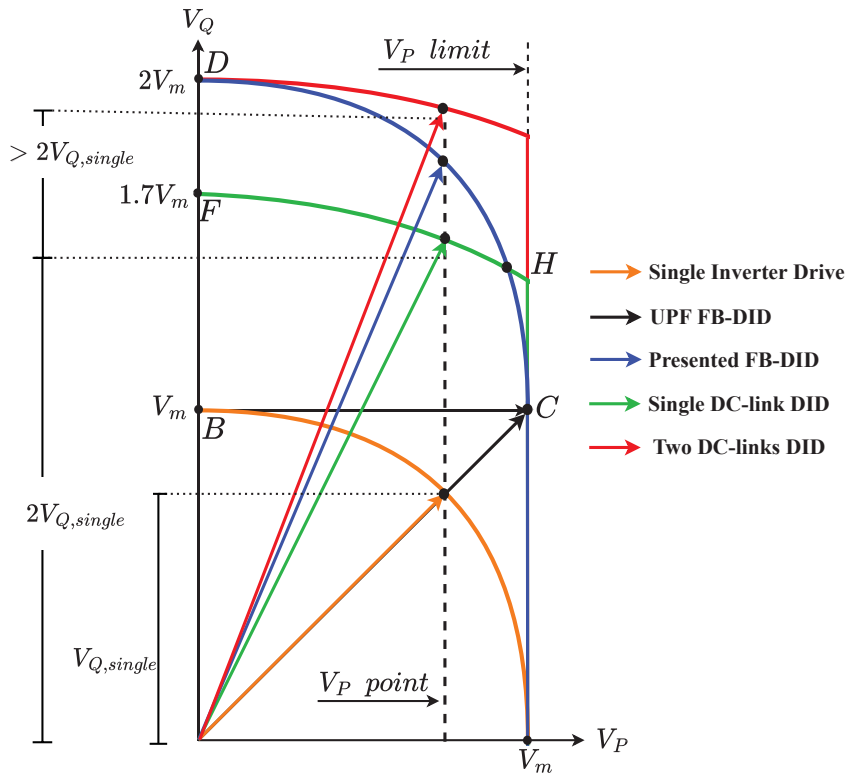

Figure 3.5: Drive's output active (V_P) and reactive (V_Q) voltage limits for a constant V_P.

Rule I:

is defined by (2.19), which states that supplying more active power (active voltage) to the motor, leads to boosting the output mechanical power (P_{mech}).

Rule II:

is defined by (2.34), which states that the more reactive voltage supplied to the motor, the more the field weakening region is extended.

Fig.3.4b, shows all the five drives active and reactive voltage limits. For a fair and more accurate comparison, the maximum DC current that has been drawn from the DC-link supply is limited to the UPF DID maximum DC current. This is applied so that all the drives have the same maximum power limit. This is achieved by limiting the active voltage component (V_P) to the maximum supplied by the UPF DID, see Fig.3.5.

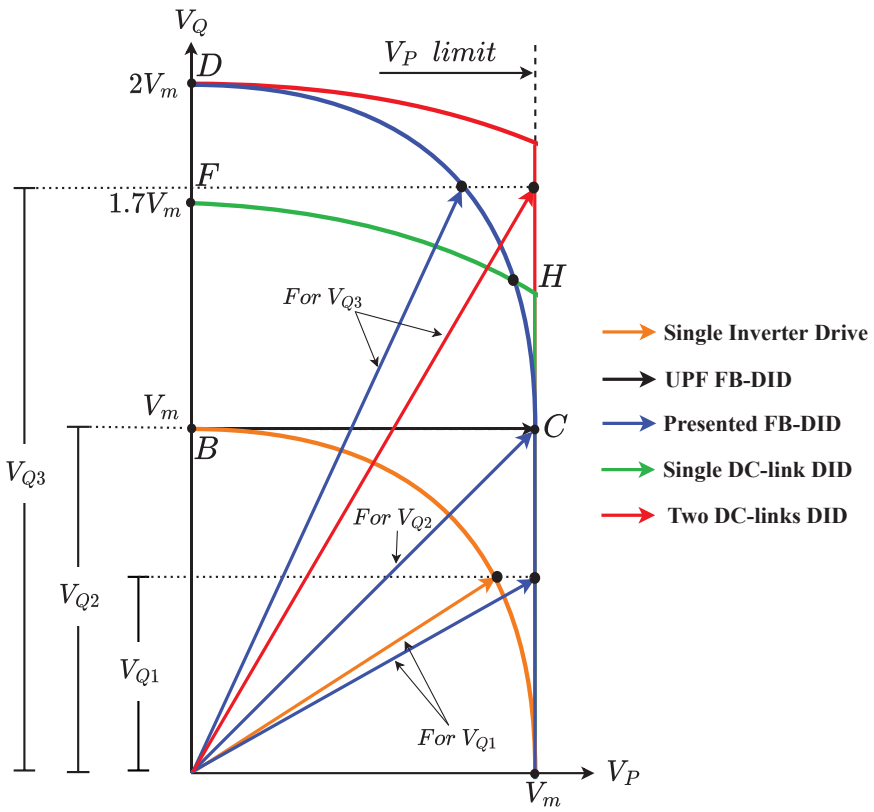

Figure 3.6: Drive's output active (V_P) and reactive (V_Q) voltage limits for a constant V_Q.

3.5 Per-Unit Speed

The per-unit speed for different drive configurations is given by ω/ω_{rated}. The per-unit speed that corresponds to $\omega = \omega_2$ is defined in this paper as the speed extension ratio (ω_2/ω_{rated}). According to *Rule II*, the more reactive voltage supplied to the IM, the higher the ω_2, and eventually the higher the drive speed extension ratio.

By taking a point on the X-axis (V_P-axis) after the V_P limit of Fig.3.5 is reached and measuring the corresponding V_Q, it is possible to predict which drive has the highest V_Q and hence the highest per-unit speed. For the V_P point of Fig.3.5, the V_P limit has been reached and then the operating point starts to move along each drive voltage curve, reducing V_P and increasing V_Q, except for UPF-DID as the operation limit is at point C.

As long as the operating point is on curve segment CD, the presented controller is expected to give higher per-unit speed than both single inverter drive and UPF DID. If the operating

point is on curve segment HD, the presented controller is expected to give higher per-unit speed than single DC-link DID. If V_Q of the presented controller is $> 2V_{Q,single}$ (see Fig.3.5), which is the case in this paper, the per-unit speed will be higher than double that of single inverter drive.

The two separate DC-links DID gives the highest output power and per-unit speed, which is expected since it has two isolated DC power sources when compared to the other drives. However, it increases the system size, cost, and complexity which is not practically desirable. The presented controller gives a per-unit speed that is close to the two separate DC-links DID because its reactive voltage is close to $2V_m$. This is a desirable feature because the presented works uses only a single DC-link and a small capacitor to achieve such a high per-unit speed when compared to two separate DC-links DID.

3.6 Output Mechanical Power

Following the same prediction principle, according to *Rule I*, the more active power, which is a function of active voltage V_P, supplied to IM, the higher the output mechanical power (P_{mech}). By taking any point on the Y-axis (V_Q-axis) and measuring the corresponding V_P, it is possible to define which drive has the highest V_P and hence the highest P_{mech}. For V_{Q1} point of Fig.3.6, the presented work, UPF, single DC-link, and two separate DC-links FW controllers have the same V_P, and produce higher V_P than that of single inverter drive. Hence, all the DIDs generate the same output power level, which is higher than that of the single inverter drive.

V_{Q2} is where the UPF DID hits it's Region II limit and moves to Region III. Hence, if the motor V_Q demand is V_{Q3} of Fig.3.6, the presented work, and two separate DC-links FW controllers are the only controllers capable of supplying that demand while remaining in Region II.[5] The two isolated DC power supplies gives higher V_P than the presented work, which means it will give higher output power. The other three FW controllers are already in Region III, which means their P_{mech} decreases as the speed increases. This means that the presented controller retains the same features of the UPF DID until point C and extends both the drive output capability and the per-unit speed after that point.

[5]Note that V_{Q1}, V_{Q2}, and V_{Q3} are three random points selected in V_Q-axis to show how the active voltage (active power) is changing for all drives for different V_Q values.

The single DC-link DID has a higher output power (higher V_P) than the presented work only between point C and H, see Fig.3.6. The presented FW controller extends both the drive output power capability and the per-unit speed after point H.

3.7 Summary

Theoretical rules are provided to explain the behaviour of the floating bridge dual inverter drive configuration in high speed regions. Based on the voltage boundary limits for different drives in stator current reference frame, the following is observed:

- The two isolated DC power supplies gives the highest voltage boost (double voltage boost of a single inverter drive), which is predictable since it has two isolated power supplies.
- The single DC power supply provides a lower voltage boost than double single inverter drive due to the circulating current elimination method.
- The presented FW controller provides the same voltage boost as the UPF dual inverter drive up to a specific operating point. After which, the presented work adds an extra voltage boost that is used to improve the drive's performance in the field weakening region.

The active power supplied to the motor is limited to the same maximum value for all drives. As a result, it is possible to compared the results of the presented work with the other drives. All dual inverter drives generate output mechanical power higher than the single inverter drive based on the voltage boundary limits in SCRF.

Chapter 4

Field Weakening Control of Dual Inverter Drives

The closed loop control strategy of a drive is an important aspect that requires investigation as it affects the performance of the drive, dynamics, and determines if the DC-link supply is fully utilized. Hence, the drive control strategy affects the drive output torque, mechanical power, speed acceleration performance, and speed extension range in field weakening region. This chapter describes the presented work speed and torque controllers together with the field weakening controller and current limits that are used to transfer from one operating region to another. Moreover, the method for the transformation from the rotor flux reference frame (RFRF) to stator current reference frame (SCRF) in the control scheme is described.

The basic principles of the single inverter drive, UPF DID, single DC-link DID, and two isolated DC-links DID FW controllers are introduced for completeness and to compared their control methodology with the presented FW controller.

4.1 Presented Field Weakening Controller

A block diagram of the presented FW controller is shown in Fig.4.1. There are two reference frames, namely the RFRF and the SCRF.

The RFRF decouples the stator current into d&q components. The rotor flux is adjusted by the d-component current and the motor torque is varied by q-component current. These two current components are tracked by two inner control loops, see Fig.4.2 with

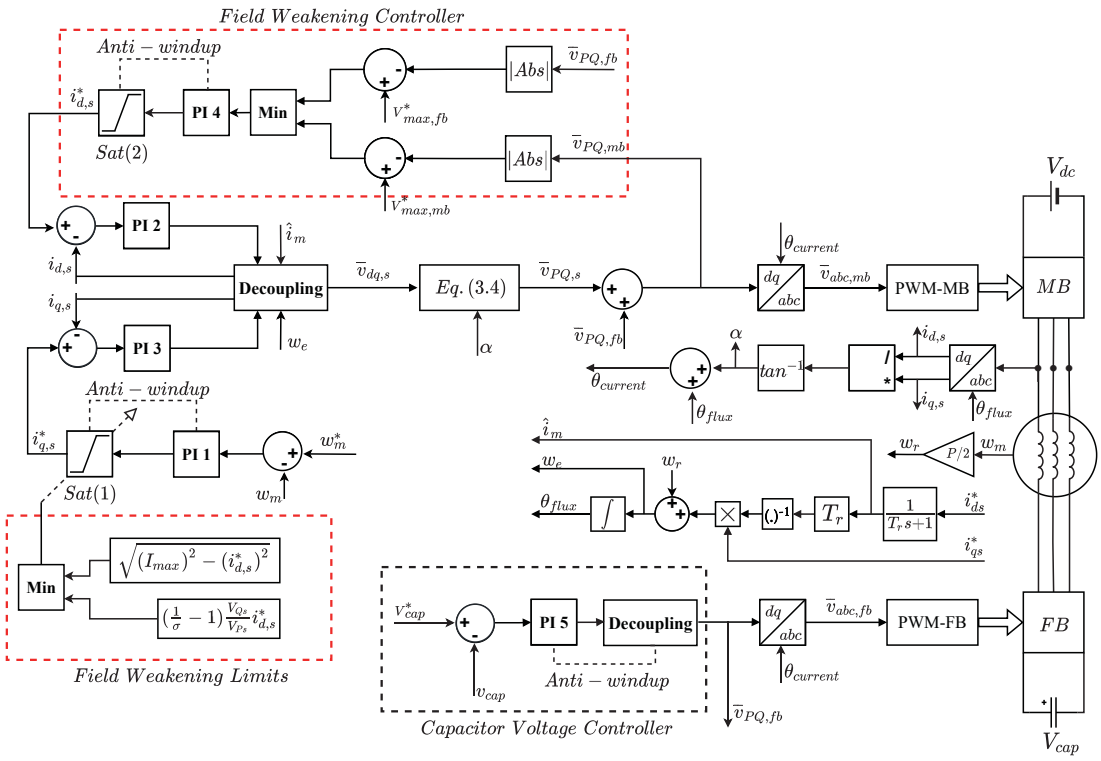

Figure 4.1: Presented field weakening controller block diagram.

d&q decoupling details while calculating $v_{d,s}$ and $v_{q,s}$, using PI 2 and PI 3. The leakage coefficient (σ) and the stator time constant (τ_s) are given by:

$$\sigma = 1 - \frac{L_m^2}{L_s L_r} \tag{4.1}$$

$$\tau_s = \frac{L_s}{R_s} \tag{4.2}$$

The two reference currents are provided by two outer control loops. The $i^*_{d,s}$ is provided by the outer flux control loop, whereas $i^*_{q,s}$ is provided by outer speed control loop.

The RFRF can be used up to the point where the stator reference voltage ($v^*_{dq,s}$) is calculated, see Fig.4.1. Once $v^*_{dq,s}$ is calculated, the transformation from RFRF to SCRF is done by the transformation matrix given by (4.3), [1].

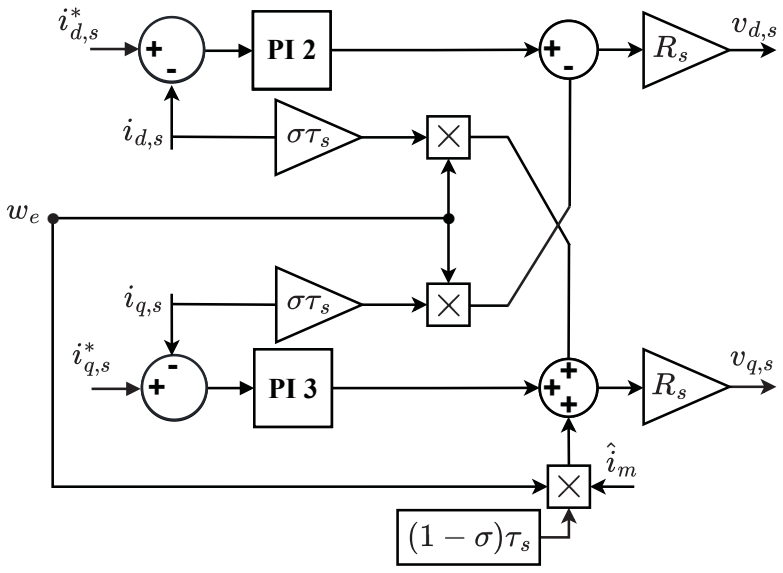

Figure 4.2: Inner current control loops.

$$\underline{v}^*_{PQ} = \begin{pmatrix} \cos\alpha & \sin\alpha \\ -\sin\alpha & \cos\alpha \end{pmatrix} \times \underline{v}^*_{dq} \tag{4.3}$$

This transformation matrix (sometimes called rotation matrix) is used to rotate a vector by a specific angle. The angle for this work is α, which is the angle between $i_{d,s}$ and $\bar{i}_s$.

The voltage references are assigned according to [1], so that at low speeds, the motor active demand is supplied by MB (MB-UPF operation), whereas motor reactive demand is supplied by FB. Hence, the angle between the MB voltage vector and the FB voltage vector is 90°, see Fig.4.3a[1]. At high speeds, the reactive requirement of the motor increases so the MB is operated at non-UPF, and the angle between $\overline{v}_{mb}$ and $\overline{v}_{fb}$ is less than 90°, see Fig.4.3b [1]. In other words, the MB and FB voltage references are as follows:

[1]The FB active voltage requirement ($v_{P,fb}$) for maintaining the capacitor charged is neglected in this figure since it is small compared to $v_{P,s}$.

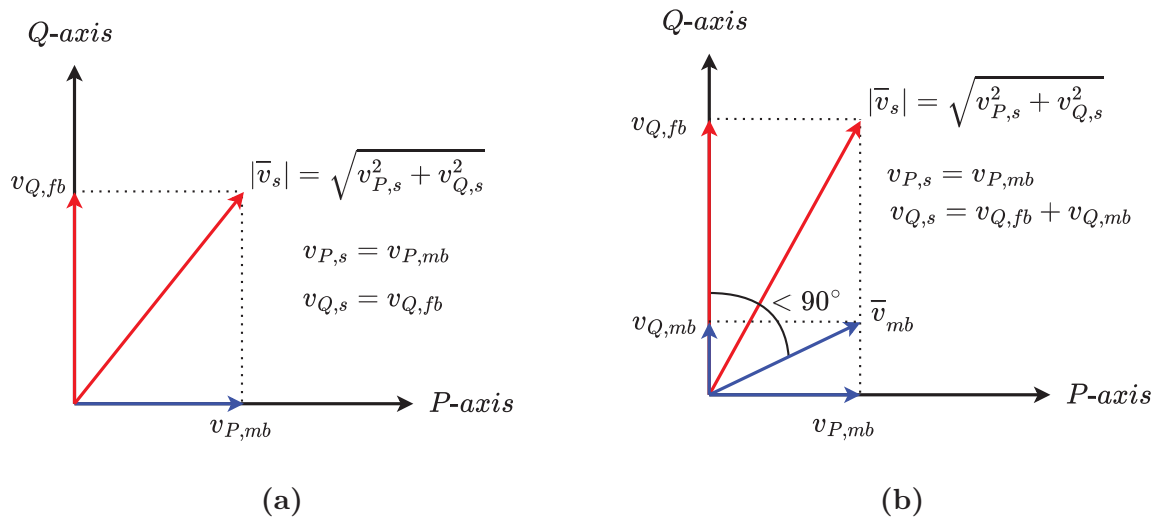

Figure 4.3: Voltage references of motor, MB, and FB: (a) At low speeds (MB-UPF operation), (b) at high speeds (MB non-UPF operation).

$$\underline{v}^*_{PQ,mb} = \begin{pmatrix} v^*_{P,s} + v^*_{P,fb} \\ v^*_{Q,s} + v^*_{Q,fb} \end{pmatrix} \tag{4.4}$$

$$\underline{v}^*_{PQ,fb} = \begin{pmatrix} v^*_{P,fb} \\ -sat(v^*_{Q,s}) \end{pmatrix} \tag{4.5}$$

where,

$$sat(v^*_{Q,s}) = \begin{cases} v^*_{Q,s} & \text{for} \quad v^*_{Q,s} < V_{max,fb} \\ V_{max,fb} & \text{otherwise} \end{cases} \tag{4.6}$$

$v^*_{P,fb}$ represents the active voltage (active power) needed to keep the capacitor voltage constant. The FB supplies the motor reactive demand as long as the $v^*_{Q,s}$ is less than the predefined maximum FB reactive voltage $v_{Q,fb}$, which is almost equal to $V_{max,fb}$ because $v^*_{P,fb}$ is really small. If $v^*_{Q,s}$ is higher than $V_{max,fb}$, the FB only supplies $V_{max,fb}$, whereas the reminder of $v^*_{Q,s}$ is supplied by the MB, see Fig.4.3b. Hence, when the motor active power requirement is high, eg. at rated torque and rated speed, the MB need to be operated at UPF to maximize the drive output power capability. This means that the FB

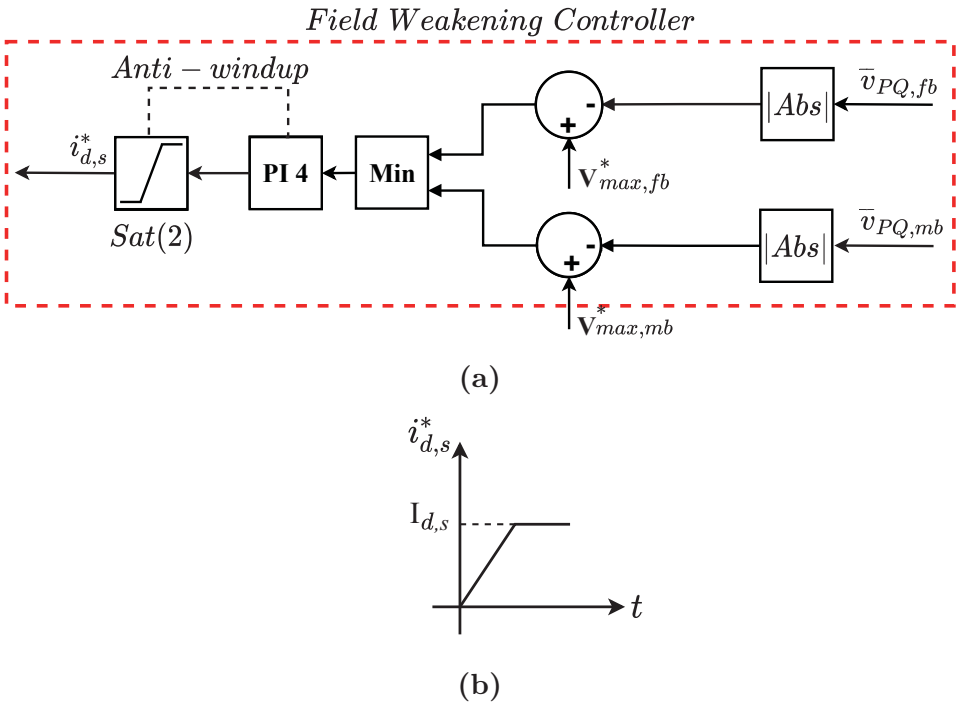

Figure 4.4: Outer flux control loop: (a) field weakening controller, (b) saturation block ($Sat(2)$) limit.

DC-link voltage should be chosen high enough so it can supply $v^*_{Q,s}$ without saturating when the motor active power requirement is high.

The MB is the only source of active power, so it will supply both the motor $v^*_{P,s}$ and the FB $v^*_{P,fb}$ in addition to any voltage reminder of $v^*_{Q,s}$ that the FB unable to supply.

The controller is equipped with the FW parts highlighted in *red* as depicted in Fig.4.1. The flux control variable ($i^*_{d,s}$) is adjusted by the outer flux control loop on the basis of the stator voltage request, see Fig.4.4a. The magnitudes of both the MB and FB voltage vectors ($|\overline{v}_{mb}|$, $|\overline{v}_{fb}|$) are compared with their corresponding maximum reference voltages ($V_{max,mb}$, $V_{max,fb}$), and the minimum error is tracked by PI controller 4. If the stator voltage request is higher than the available voltage of the MB or FB, the flux is reduced; otherwise, it is kept at rated value by the saturation block [$Sat(2)$]. The limit of this saturation block is shown in Fig.4.4b.

The speed is controlled by PI 1 and the reference current ($i^*_{q,s}$) is provided to the inner q-axis current control loop, Fig.4.5a. This current is limited by the saturation block

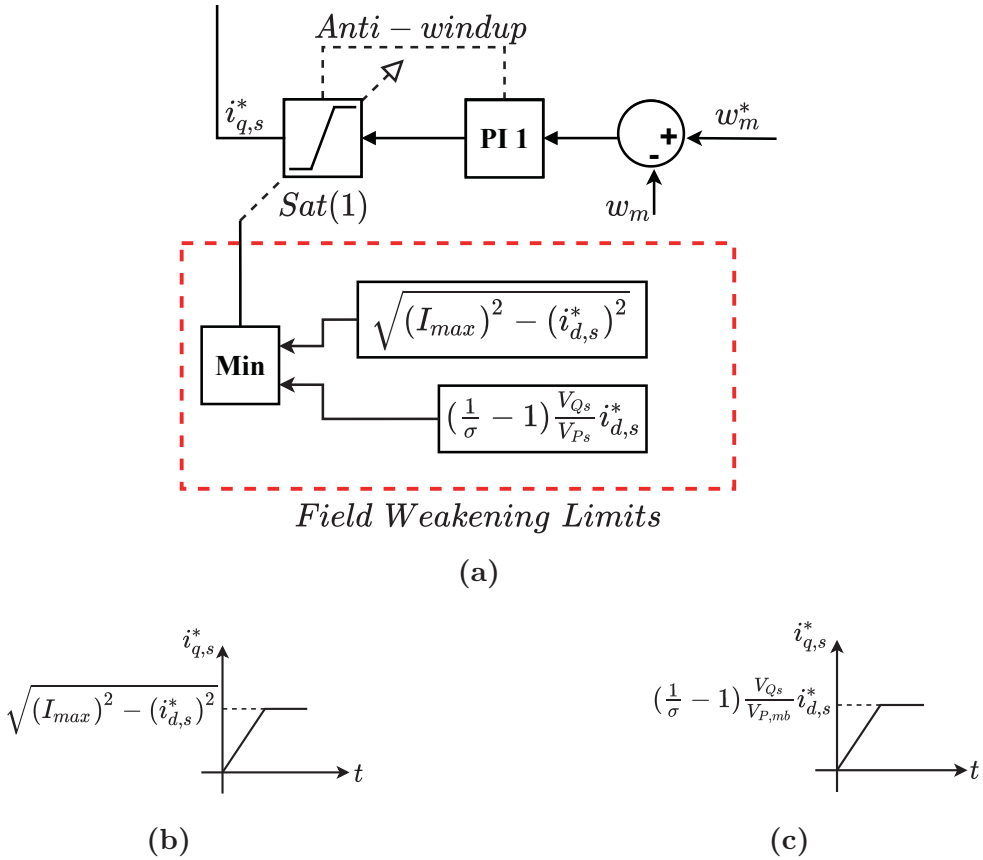

Figure 4.5: Outer speed control loop: (a) speed controller, (b) saturation block ($Sat(1)$) Region I and II limit, (c) saturation block ($Sat(1)$) Region III limit.

$[Sat(1)]$, which has two field weakening limits and ensures that the maximum current constraints are met by ensuring that $i_{q,s} = \sqrt{I^2_{max} - i^2_{d,s}}$ in both Regions I and II, whereas $i_{q,s} = (\frac{1}{\sigma} - 1)\frac{V_{Qs}}{V_{Ps}} i_{d,s}$ in Region III. These two limits are shown in Fig.4.5b and Fig.4.5c. The first limit takes place in Region I, where $i_{d,s}$ is held constant at rated value. Hence, for having the maximum phase current (I_{max}), $i_{q,s}$ is held constant at rated value, which as a result gives the rated constant torque in Region I. The same limit takes place in Region II, where $i_{d,s}$ is decreasing, so $i_{q,s}$ is increasing for maintaining the same I_{max}.

The second limit takes place in Region III. As discussed before, in order to increase the speed in Region III above ω_2, the phase current is decreased as the speed is increasing [2]. For achieving this, the second limit forces $i_{q,s}$ to decrease as the speed is increasing in Region III. Since both $i_{d,s}$ and $i_{q,s}$ are decreasing, the phase current decreases as the

[2]See subsection 2.4.3.

operating frequency increases in Region III. Both limits satisfy the FW operation current constraints and produce the maximum torque.

The capacitor reference voltage is compared to the feedback voltage and the error is tracked by PI 5, Fig.4.1, and decoupled from the motor transients using the decoupling scheme presented by [13].

4.2 Main Bridge Unity Power Factor

The implemented UPF controller has the same concept as the one carried out by [31], also reported in [30], [33], [40], and [42], (MB UPF operation concept). The voltage references for this scheme are assigned so that the motor active demand is supplied by MB, while the motor reactive demand is only supplied by FB. In other words, the MB and FB voltage references are as follows:

$$\underline{v}^*_{PQ,mb} = \begin{pmatrix} v^*_{P,s} + v^*_{P,fb} \\ 0 \end{pmatrix} \tag{4.7}$$

$$\underline{v}^*_{PQ,fb} = \begin{pmatrix} v^*_{P,fb} \\ -v^*_{Q,s} \end{pmatrix} \tag{4.8}$$

4.3 Single Inverter Drive

The implemented single inverter drive controller basic principle is presented in [8]. The inverter maximum reference voltage is compared with the magnitude of voltage requested by the motor and the error is passed to a FW regulator to adjust the field level, Fig.4.6. The implemented limitations ensure that the maximum current constraints are met by ensuring that $i_{q,s} = \sqrt{I^2_{max} - i^2_{d,s}}$ in both Region I and II, whereas $i_{q,s} = \hat{i_m}/\sigma$ in Region III. Hence, the implemented limitations are simple and do not require an additional regulator as in [10].

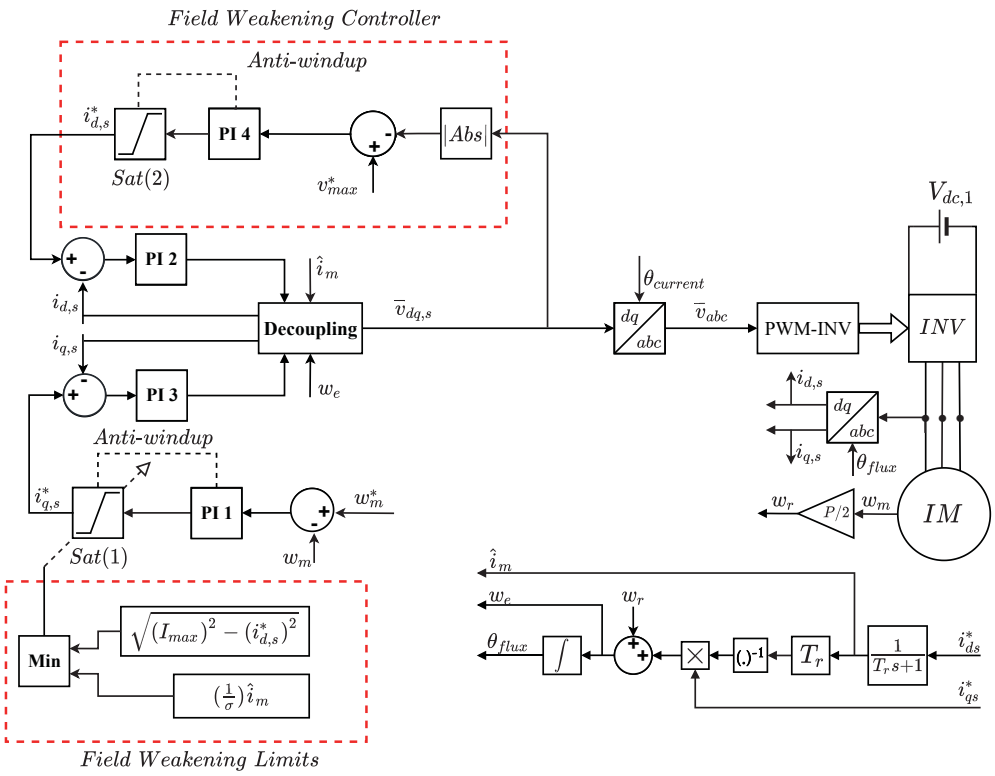

Figure 4.6: Single inverter drive field weakening controller block diagram.

4.4 Two Isolated DC Power Supplies

The motor active voltage demand is controlled independently by comparing the stator active voltage request ($v_{P,s}$) with the required reference value. Then, the minimum error is passed to a FW regulator to adjust the field level, Fig.4.7.

The angle between the first inverter voltage vector ($\overline{v}_{inv1}$) and the second inverter voltage vector ($\overline{v}_{inv2}$) is 180 degree for having the maximum fundamental phase voltage, Fig.4.8a. The motor real and reactive power demand is equally shared between the two inverters. The vector addition of both inverter 1 and inverter 2 is shown in Fig.4.8b.

The total stator voltage is given by:

$$\overline{v}_s = \overline{v}_{inv1} - \overline{v}_{inv2} \tag{4.9}$$

The outer speed control loop provides the q-axis current reference to the inner q-axis

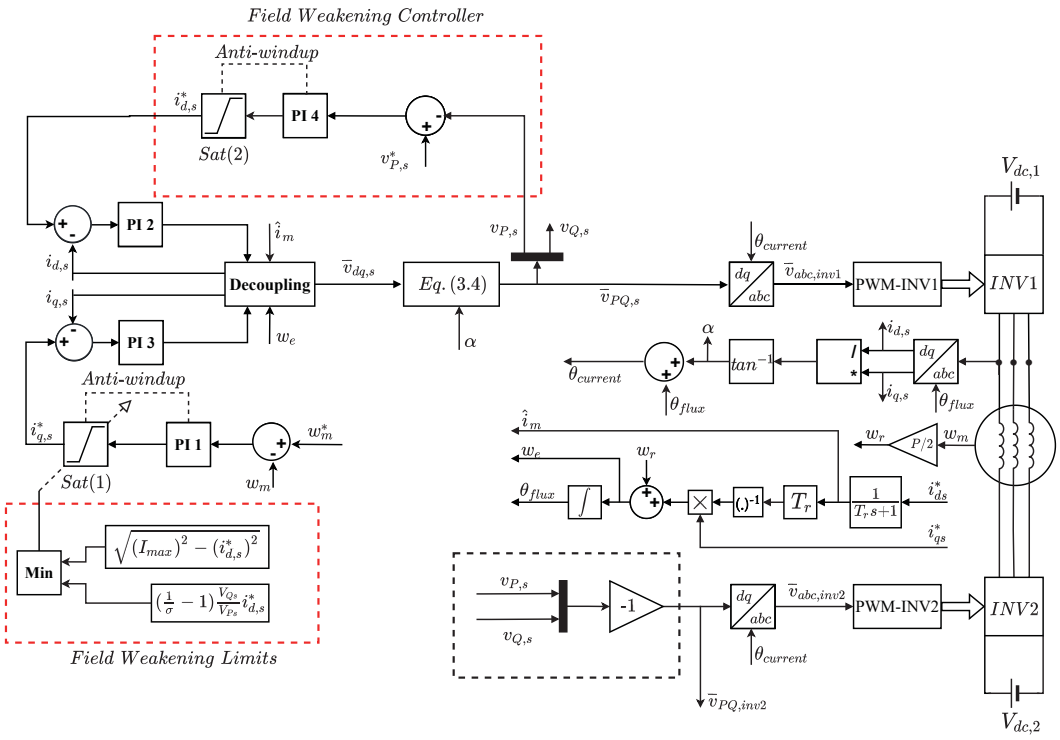

Figure 4.7: Two isolated DC power supplies field weakening controller block diagram.

current control loop, Fig.4.7. This q-axis current reference is limited by two FW limits. The first FW limit ensures that the phase current is at the maximum by ensuring that $i_{q,s} = \sqrt{I_{max}^2 - i_{d,s}^2}$ in both Regions I and II. This FW limit is common for all FW drives since they all maintain the maximum phase current in both Region I and II. The second FW limit ($i_{q,s} = (\frac{1}{\sigma} - 1)\frac{V_{Qs}}{V_{Ps}} i_{d,s}$) ensures that the q-axis current is decreasing as the speed is increasing in Region III, which as a results decreases the overall phase current. Notice that the second FW limit is similar to that derived for the presented work. This is because the derived second FW limit (2.38) is only a function of the reactive and active voltage supplied to the IM. Hence, it can be applied for different DIDs other than the presented FW controller.

4.5 Single DC Power Supply

The motor active voltage demand is controlled independently by comparing the stator active voltage request ($v_{P,s}$) with the required reference value similar to that of two isolated

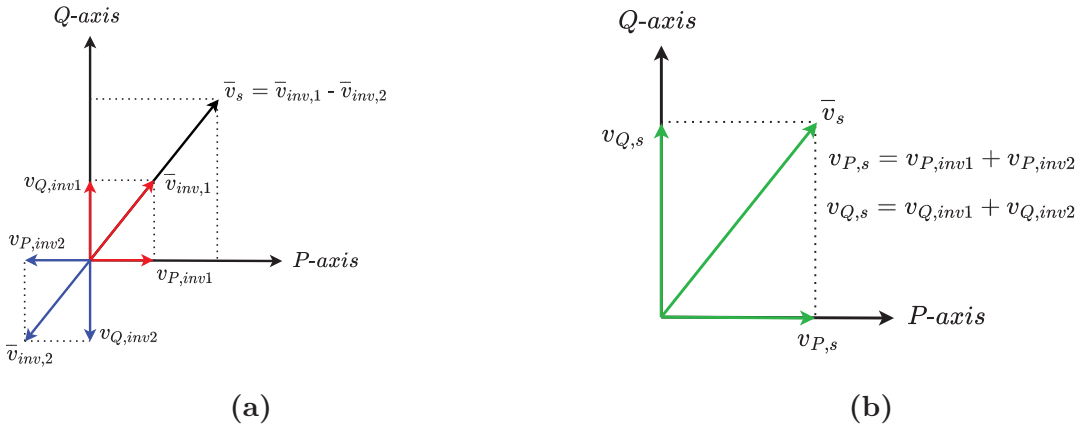

Figure 4.8: Two isolated DC power supplies voltage vectors of: (a) motor, inverter 1, and inverter 2, (b) vector addition of $\overline{v}_{inv1}$ and $\overline{v}_{inv2}$ to give overall $\overline{v}_s$.

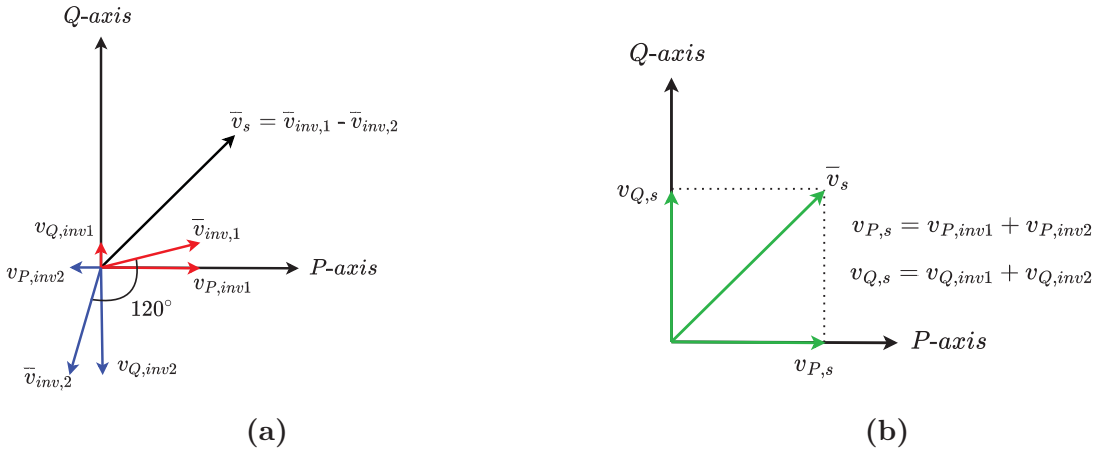

Figure 4.9: Single DC power supply voltage vectors of: (a) motor, inverter 1, and inverter 2, (b) vector addition of $\overline{v}_{inv1}$ and $\overline{v}_{inv2}$ to give overall $\overline{v}_s$.

DC power supplies. Then, the minimum error is passed to a FW regulator to adjust the field level, Fig.4.7. The only different from the two isolated DC power supplied FW controller is that the single DC power supply suffers from circulating currents, hence a zero sequence circulating current suppression method need to be implemented.

The implemented circulating currents suppression method is presented in [21]. According to [21], the zero sequence circulating currents can be canceled out with the subtractive property of the phase voltage if the angle between the first inverter voltage vector ($\overline{v}_{inv1}$) and the second inverter voltage vector ($\overline{v}_{inv2}$) is reduced from 180 to 120 degree, Fig.4.9a.

This method basic concept is to make inverter 1 and inverter 2 always taking the same

PWM signals which leads to the identical CMVs of the two inverters. This identical CMV of both inverters cancels out with the subtractive property of the phase voltage. More details can be found in [21].

The total stator voltage is given by (4.9). Unlike the two isolated DC-links DID, the motor power is not shared equally between the two inverters, see Fig.4.9a, if the conventional zero sequence circulating current suppression method described in [21] is implemented. It can be clearly seen that the first inverter (v_{inv1}) supplies the majority of the active voltage and hence the active power, whereas the second inverter (v_{inv2}) supplies the majority of the reactive voltage (reactive power). The is undesirable as the power losses will not be shared equally between the two inverters. However, this is out of the scope of this thesis as the focus is on the single DC power supply DID FW operation. The vector addition of both inverter 1 and inverter 2 to give the overall motor vector is shown in Fig.4.9b.

4.6 Summary

A field weakening control scheme is presented that boosts the field weakening region range of a dual inverter drive using a floating capacitor bridge along with other four field weakening control schemes for a single inverter drive, UPF-DID, single DC supply DID and two isolated DC supplies DID. The control references have been assigned so that the main bridge connected to the main DC supply is operated at UPF at low speed, whereas the floating bridge supplies the motor reactive power demand. At high speeds, the main bridge is operated at non-UPF and used to supply some reactive demand after the floating bridge reaches its maximum limit. Furthermore, two field weakening torque current limits are discussed. The first torque current limit takes place in both Region I and Region II to ensure the maximum phase current is maintained for maximum torque operation. The second torque producing current limit takes place in the decreasing power region to decrease the overall phase current. As a result, the speed can further be increased in this region.

Chapter 5

Results

A simulation and an experimental prototype was used to illustrate the features of and to validate the proposed controller. Transient, steady state, speed acceleration, and maximum fundamental stator voltage results are obtained and compared for different drives.

The motor parameters used experimentally and for simulation are given in Table 5.1. The original base speed of the motor is 1760 rpm and its maximum possible speed is 5800 rpm, which is about 3.3 times the base speed. If the original base speed of the motor is used, it is not possible to test the five drives FW operation, because for example, the single inverter drive speed extension ratio is 4 times the base speed ($4 \times 1760 = 7040rpm > 5800rpm$), which is higher than motor allowable max speed. Hence, the motor base speed is lowered to 480 rpm by lowering the machine line voltage below the rated value. This allow the speed range extension of the controllers to be tested without exceeding the limitations of the laboratory experimental motor and dynamometer. The 480 rpm base speed has also been selected because it allows for an operation range up to 12 p.u speed, which is enough to show the system performance in Region I, Region II, and Region III.

5.1 Simulation Results

The presented scheme has been implemented in PLECS environment with the system parameters that are given in Table 5.1.

Table 5.1: System Parameters

Parameter	**Symbol**	**Value**
Stator resistance	R_s	0.466 Ω
Rotor resistance	R_r	0.2873 Ω
Stator leakage inductance	L_{ls}	3.03 mH
Rotor leakage inductance	L_{lr}	2.02 mH
Magnetizing inductance	L_m	47 mH
Number of poles	p	4
Rated power	P_{rated}	0.85 KW
Rated speed	N_{rated}	480 rpm
Rated torque	T_{rated}	17 N_m
Moment of inertia	J	0.0279 $kg\ m^2$
Rated current	I_{rms}	13.6 A
Rated line voltage	V_{rms}	76 V
Floating bridge capacitance	C	120 μF
Main DC link voltage	$V_{DC,mb}$	108 V
Floating DC link voltage	$V_{DC,fb}$	108 V
Switching frequency	f_s	10 kHz

5.1.1 Voltage Vectors

Presented Controller

The X-Y plots, Fig.5.1, show the presented controller motor demand in SCRF, the voltage in SCRF supplied by both the MB, and the FB. Combining the MB voltage vector with the FB voltage vector gives the overall IM voltage vector that is shown in Fig.5.1a. The three speed points, ω_a, ω_b, and ω_2, in Fig.5.1a are added to show how the IM voltage vector changes as the speed increases. Note that the FB voltage in SCRF, Fig.5.1c, neglects the active voltage absorbed by the FB to keep the capacitor charged because it is small compared to the active voltage absorbed by the motor.

Initially, the motor reactive demand is fully supplied by the FB, allowing the MB to be operated at UPF, see Fig.5.1b & Fig.5.1c. As the operating frequency increases, the IM reactive demand increases. The point where the FB hits its maximum reactive voltage limit ($V_{max,fb}$) is defined by point C in Fig.5.1c. This operating point is corresponding to point C of Fig.3.1a. After that point, the FB can not supply any reactive demand, so the MB is operated at non-UPF and used to supply some reactive demand by reducing

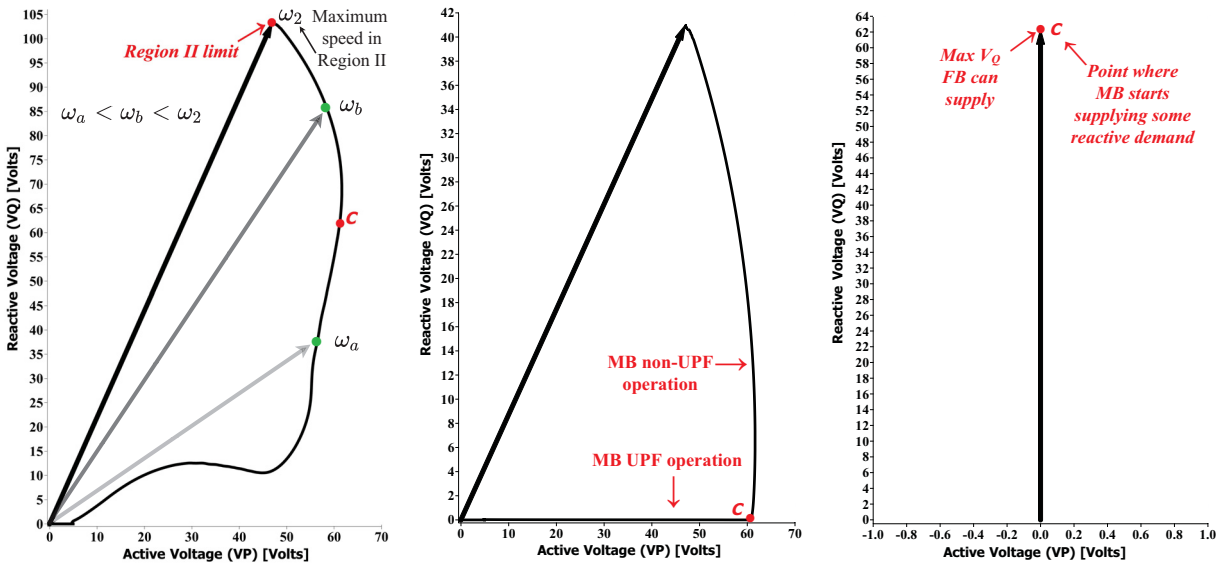

Figure 5.1: Presented controller voltage vectors in SCRF: (a) IM active (V_P) and reactive (V_Q) voltage demand, (b) MB output voltage vector, and (c) FB output voltage vector.

V_P and increasing V_Q, see Fig.5.1b. This corresponds to the MB vector moving along the boundary-segment CD of Fig.3.1a. Finally, when V_P of the MB is reduced to be equal to IM rated value when operated using single inverter drive ($V_{P,rated} = 46V$, for this scenario), the presented FW controller hits its Region II limit with a speed equal to ω_2 and moves to Region III, see Fig.5.1a.

The MB voltage vector is kept constant in Region III and hence the stator voltage vector is kept constant as well, see Fig.5.1. The stator voltage vector magnitude in Region III is about 113V, see Fig.5.1a, which is about 1.82 times the single inverter drive voltage vector magnitude as shown in section 5.2. The presented controller satisfies the voltage constraints of both the MB and the FB as the voltage vector magnitude is always less than the bridge maximum voltage.

In SCRF, the motor phase current vector is considered as the P-axis. In other words, any voltage component aligned with the motor phase current is an active voltage whereas any voltage component 90° leading the phase current is a reactive voltage. Fig.5.2 shows stator, MB and FB voltages along with the phase current in SCRF [1]. Since the phase current is considered as the P-axis, the active component of this current ($i_{P,s}$) will be

[1]Note that $v_{P,fb}$ is ignored in this figure. Hence, $\overline{v}_{fb}$ is given by $v_{Q,fb}$.

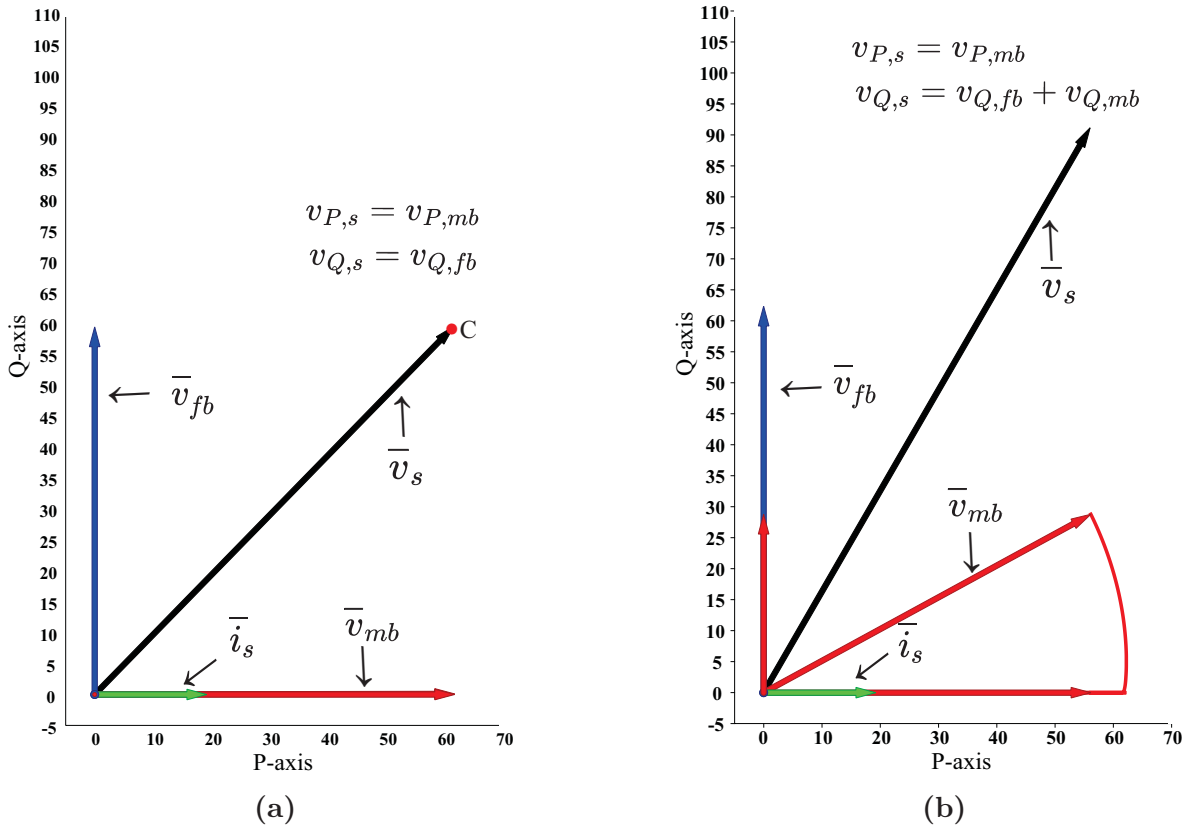

Figure 5.2: Presented controller SCRF voltage and current vectors: (a) MB supplies only active voltage (power) demand, (b) MB supplies some reactive voltage (power) demand.

equal to the magnitude of the stator current (I_{max}), whereas $i_{Q,s}$ is equal to zero, see Fig.5.2a [2]. At point C or before, Fig.5.2a, the MB voltage vector is in phase with the stator active current component and FB voltage vector is 90° leading it. After point C, Fig.5.2b, the MB voltage vector is leading the phase current to supply some reactive power demand (angle between MB and FB is less than 90°). Fig.5.2b is at higher speed than Fig.5.2a since the MB is supplying some reactive demand. Note that the FB absorbs a small amount of active power (active voltage) for keeping the capacitor charged, see Fig.5.3 [3].

The MB-UPF DID voltage vectors behavior is similar to that of Fig.5.2a as point C represents the maximum voltage that drive can supply.

[2] $I_{max} \approx 19A$.
[3] $V_{P,fb} < 1V$, which is really small compared to that absorbed by motor.

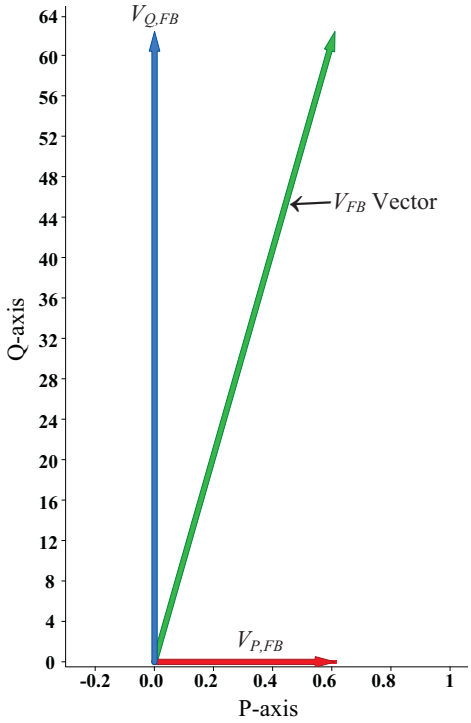

Figure 5.3: Real voltage (power) absorbed by FB to keep the capacitor charged.

Two Isolated DC Power Supplies

The voltage in SCRF of the IM, INV1, and INV2 is shown in Fig.5.4a. The overall IM stator voltage is given by (4.9)[4]. As can be seen, both inverters show similar behavior and equally share the overall motor voltage demand. The angle between both inverters voltage vectors is 180°. The overall active voltage supplied by both inverters is limited to the maximum active voltage supplied by the MB-UPF DID, so that this drive draws the same dc power as the MB-UPF DID.

Single DC Power Supply

The motor demand in SCRF supplied by both INV1 and INV2 is shown in Fig.5.4b. Since this drive suffers from circulating currents, the angel between both inverters is reduced from 180° to 120°, which as a result reduces the supplied fundamental voltage by 15%

[4] This formula is repeated here for convenience: $\overline{v_s} = \overline{v}_{inv1} - \overline{v}_{inv2}$

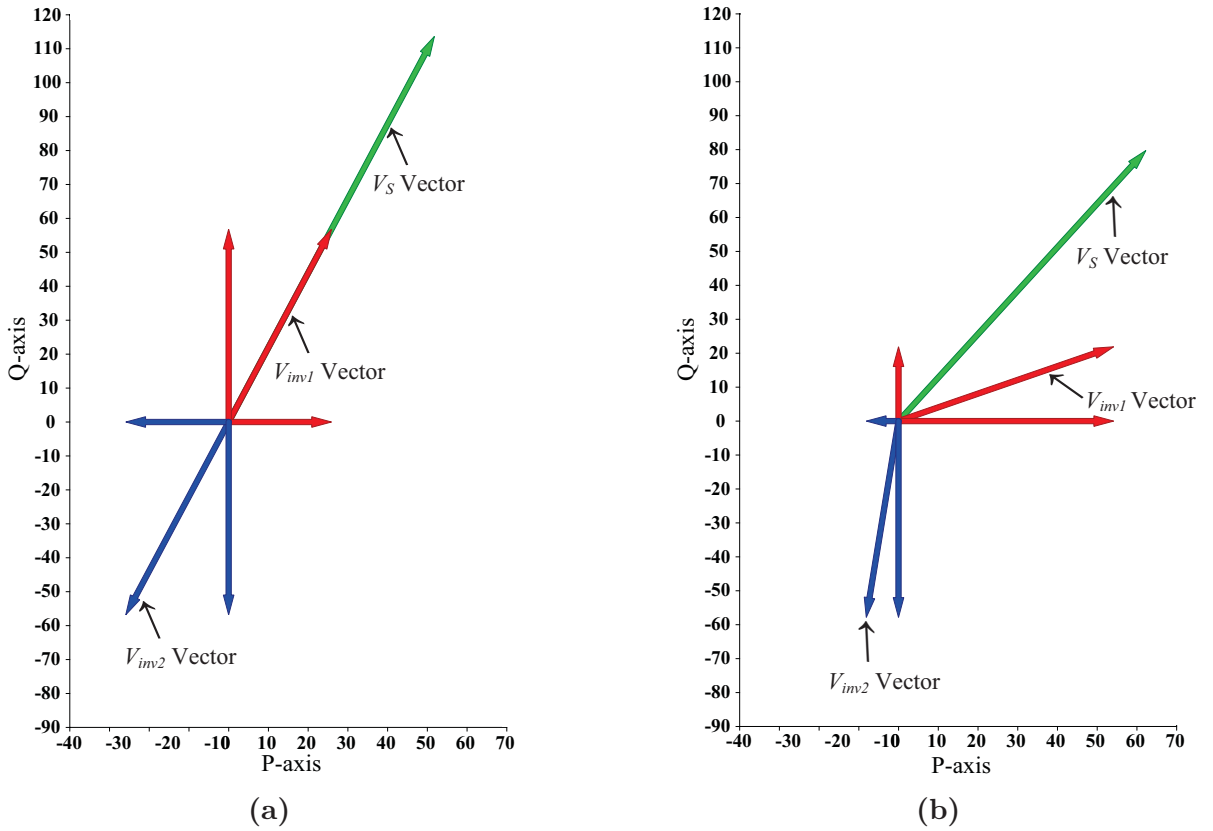

Figure 5.4: Voltage vectors in SCRF: (a) Two isolated DC power supplies, (b) single DC power supply.

[21]. As a result of 120° phase difference between both inverters, the power demand of IM is not shared equally between both inverters. One inverter supplies the majority of active voltage (active power) demand of motor, whereas the other inverter supplies the majority of reactive demand, see Fig.5.4b. The overall stator voltage vector is given by (4.9).

5.1.2 Field Weakening Limits

Presented Controller

As described in Section 4.1, there are two FW limits that are used to transfer from one operating region to another. The minimum of those two limits is passed to *Sat(1)* to control $i^*_{q,s}$, see Fig.4.1. The performance of these FW limits is shown in Fig.5.5. Both FW limits are shown in Fig.5.5a and the minimum of these two limits is shown in Fig.5.5b.

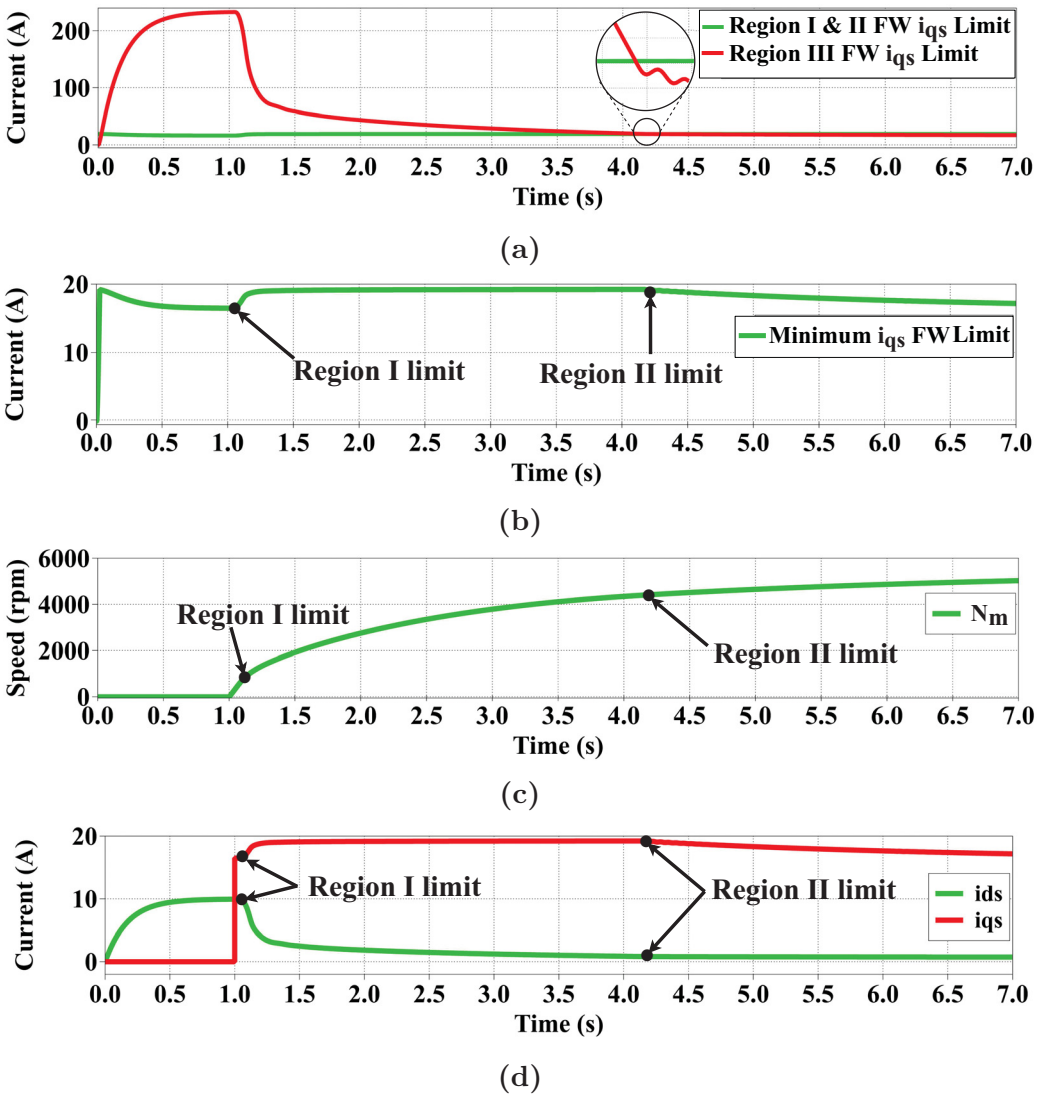

Figure 5.5: Presented controller field weakening limits performance for a speed step from 0 to 8000 rpm at $t = 1$ sec: (a) Region I,II, and III FW limits, (b) minimum of both FW limits, (c) rotor speed, and (d) d&q stator currents.

Initially, between t = 0-0.5 sec, the motor flux is being increased to the rated value. Then, at t = 1sec, a stepped increase in speed demand from 0 to 8000 rpm is applied, which initiates Region I. In this region, the minimum limit is maintained constant, keeping the torque current ($i_{q,s}$) constant, see Fig.5.5b & Fig.5.5d. Then, in Region II, the flux current ($i_{d,s}$) decreases, so the minimum limit increases torque current to maintain the rated phase current. Finally, in Region III, the minimum limit is decreasing, which as a result, forces the torque current to decrease as the operating frequency increases, see Fig.5.5. Since

both the $i_{d,s}$ and $i_{q,s}$ are decreasing in Region III, the phase winding current decreases.

Furthermore, as can be seen from Fig.5.5d, at Region II limit, the flux current is almost zero, it is exactly $i_{d,s} = 0.8A$, and $i_{q,s} \cong I_{max} \cong 19A$, which validates the assumption that has been made in (2.34).

5.2 Experimental Results

The three drive configurations have been realized experimentally to verify the feasibility of their control schemes. The PLECS RT Box platform is used to implement the drive's control schemes. The MAGTROL DSP 6000 dynamometer is used to load the IM. The experimental setup is shown in Fig.5.6. For a fair and more accurate comparison, the same experimental platform is used for all schemes.

5.2.1 Transient Behavior

Fig.5.7 shows the acceleration transient of the IM with the presented FW controller for a speed step to 6000 RPM (transient end is not visible). Initially, the motor is magnetizing, the flux current is increased to the rated value. The torque current increases rapidly after the speed step is applied, increasing the rotor speed. As soon as Region I limit has been reached, the FW PI controller[5] decreases the flux current while slightly increases the current $i_{q,s}$ to keep the phase current (I_{phase}) at the maximum rated value as shown in Fig.5.7a. When the FB hits its maximum reactive voltage at point C, Fig.5.1, the MB starts to supply some reactive demand and its voltage vector moves along curve segment (CD) of Fig.1.1ba, decreasing active component and increasing the reactive component. This explains why the MB PF curve decreases below unity after point C, see Fig.5.7b. Finally, when the FB is at its maximum and the MB can not decrease the active voltage to supply more reactive voltage, the drive hits its Region II limit.

During the field weakening operation and the transition from one region to another, the FB capacitor voltage is kept constant and decoupled from the motor transients as depicted in Fig.5.7b. The operation point where the MB PF starts to behave almost in a linear

[5]PI 4 in Fig.4.1.

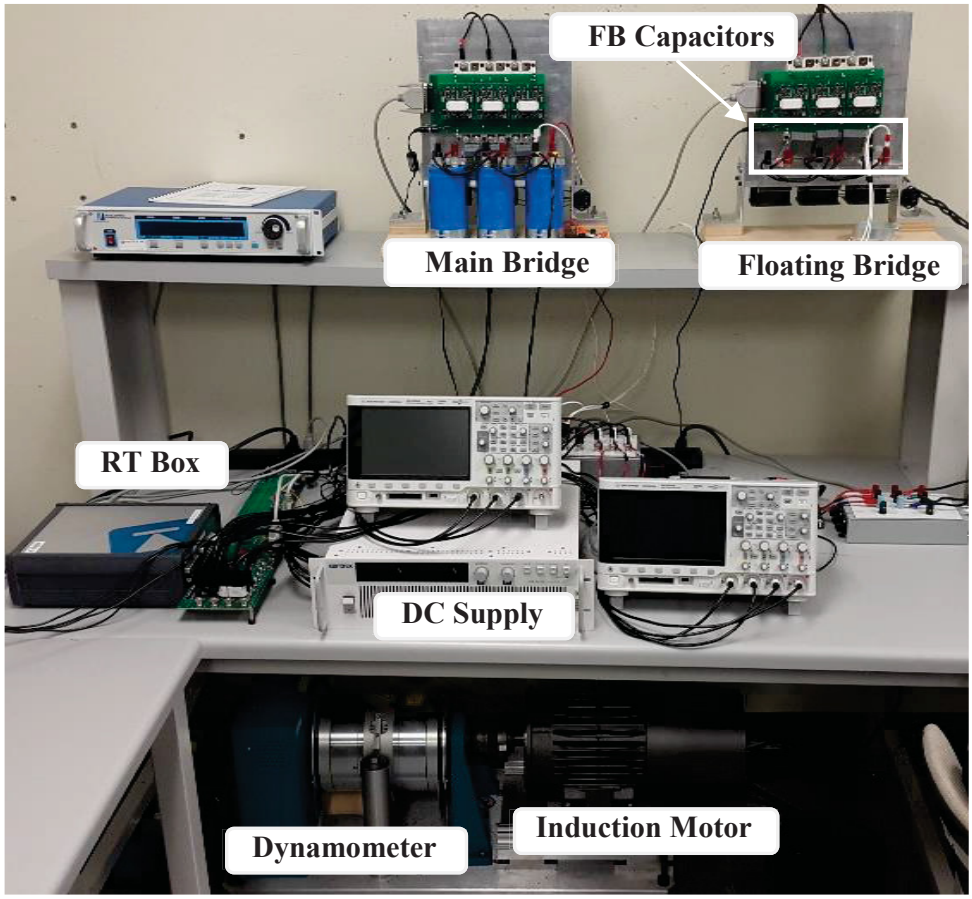

Figure 5.6: Experimental setup with 120 μF floating bridge capacitance.

manner defines Region II speed limit, see Fig.5.7b. The maximum fundamental voltage applied to the motor for the presented FW controller is also shown in Fig.5.7b. As can be seen, the maximum fundamental stator voltage is about 112V. Moreover, the phase current is kept constant at the maximum rated value in Region I and Region II for the maximum torque operation, whereas it is decreasing in Region III to further increase the motor speed. Also, at Region II limit, $i_{d,s} \cong 0.83A$, which also validates the assumption of equation (2.34) experimentally.

Since the motor phase current is decreasing at Region III to further increase the speed beyond Region II speed limit, the active power supplied to the motor decreases with the phase current. This explains why the speed acceleration performance is lower after Region II limit. The motor accelerates from 0 to $\approx$ 4200 rpm in almost 2.82 seconds before Region II limit, whereas the motor accelerates from 4200 to $\approx$ 5700 rpm in almost 8.7 seconds in

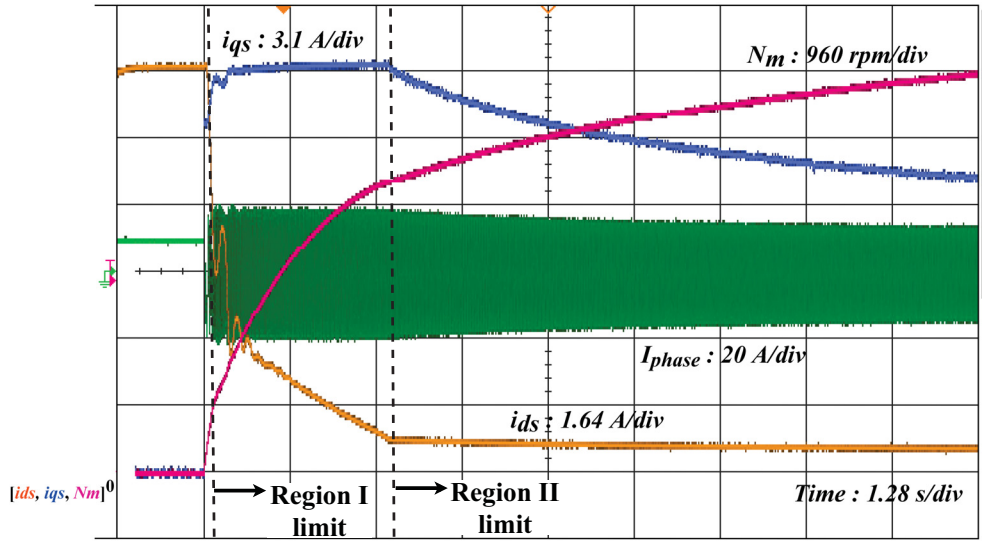

(a)

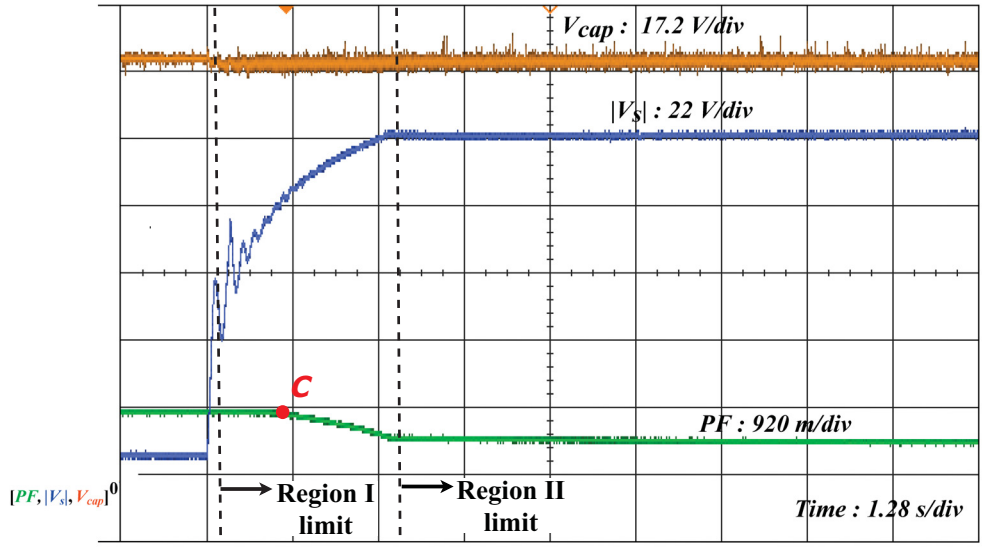

(b)

Figure 5.7: Transient behavior of presented FW controller for a speed step to 6000 RPM. (a) Motor phase current, $d\&q$ currents, and rotor mechanical speed, (b) motor stator voltage magnitude, FB capacitor voltage, and MB power factor.

Region III.

As can be seen from Fig.5.8, once the motor accelerates to the speed set point, 3000 rpm, the torque current ($i_{q,s}$) decreases to the value required to drive the motor at a 3000 rpm with a torque of 0.3 p.u ($\approx$ 5 Nm), whereas the flux current ($i_{d,s}$) is held constant at

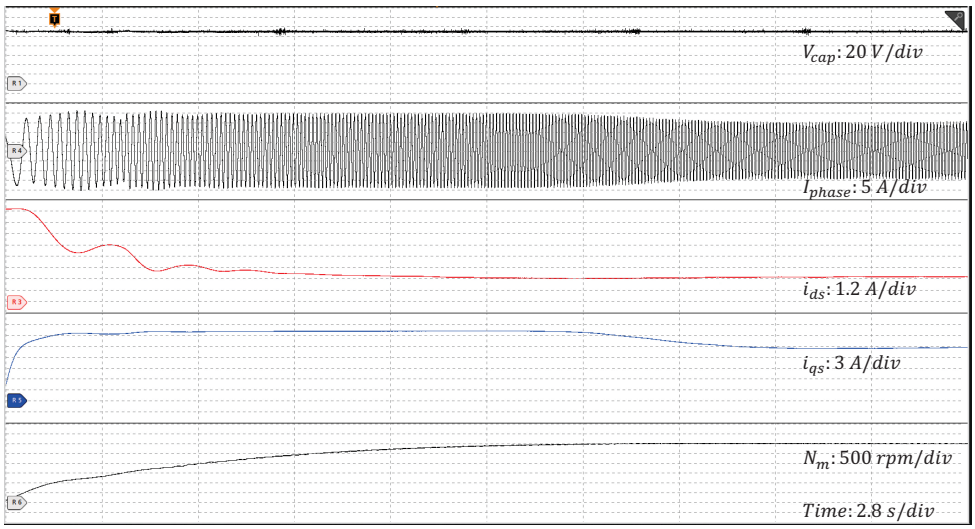

Figure 5.8: Motor acceleration performance to a speed in Region II, from 0 to 3000 rpm, while a 0.3 p.u. torque is applied by the dynamometer.

the value where the speed set point has been reached. The capacitor is held constant as the motor transfer from Region I to Region II and as the motor transfer from transient behaviour to the steady state behaviour.

5.2.2 Steady State Behavior

Fig.5.9 shows the experimental steady state power and torque capability of the presented controller as a function of motor rated values ($P_{mech,rated}$, $T_{e,rated}$, ω_{rated}) with Region I and Region II speed limits being defined by *blue* points. The MB steady state PF of the presented controller is also shown in Fig.5.9c.

In Region I, the torque is held constant at the rated value, so the output mechanical power is increasing with the speed ($P_{mech} = T_e \times \omega_m$), see Fig.5.9a and Fig.5.9b. After Region I limit, the flux is weakened, so the torque is decreasing as the speed is increasing. The MB is still operating at UPF at the beginning of Region II, see Fig.5.9c, hence the output mechanical power is kept constant up to point C of Fig.5.9a. The controller presented after point C decreases MB active component and increases reactive component. This explains the behavior of output mechanical power and MB PF curves. Both are decreasing as the active component decreases, see Fig.5.9a and Fig.5.9c.

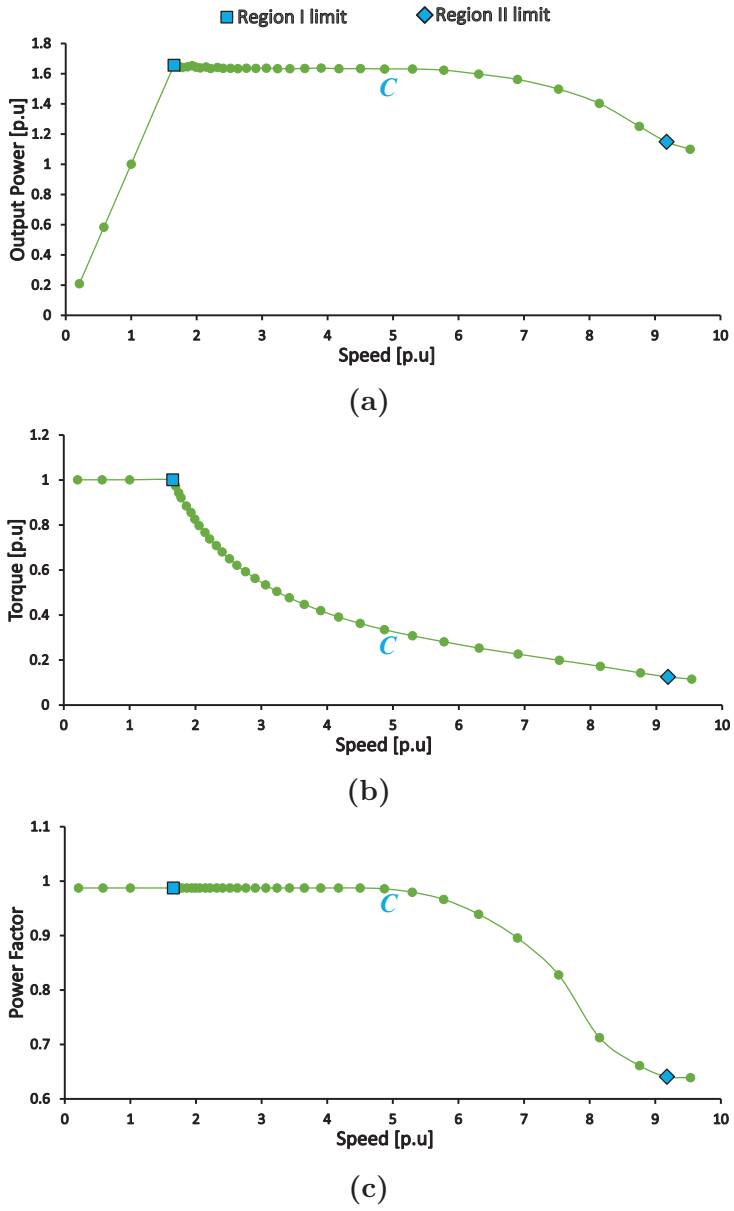

Figure 5.9: Experimental steady state behavior of the presented controller. (a) Output steady state power curve, (b) steady state torque curve, and (c) main bridge power factor curve.

Fig.5.10 compares the experimental steady state power and torque capabilities of the five drives as a function of motor rated values ($P_{mech,rated}$, $T_{e,rated}$, ω_{rated}) with Region I and Region II speed limits being defined by *blue* points. The maximum DC current being drawn from the power supply for all drives is limited to maximum current value of UPF DID.

As can be seen, the five drives predicted behavior by Fig.3.5- Fig.3.6 can be clearly observed. The presented controller retains the same torque and power boost capability of the UPF DID until point C and extends the drive output capabilities after point C, see Fig.5.10a.

Despite the non-UPF operation of the presented approach after point C, its output power is still higher than UPF DID output power. This is because, on one hand, after point C, the UPF DID is already in Region III, which means its output power is decreasing as the speed is increasing. The presented approach, on the other hand, is still in Region II after point C, but moves from UPF to non-UPF operation in an optimized manner. In other words, the presented approach after point C decreases the MB supplied active power only by the amount of the reactive power needed by the motor that cannot be supplied by the FB, which results in the maximum output power possible. Hence, both DIDs decrease their output power after point C, see Fig.5.10a. However, the rate of output power decrement because the UPF DID is in Region III is much higher than the rate of output power decrement because the optimized non-UPF operation of the presented approach. This results in a higher output power for the presented approach.

The speed extension ratio (ω_2/ω_{rated}) is the speed that corresponds to Region II limit of Fig.5.10. The speed extension ratio of the UPF drive is 5, whereas it is 9.2 for the controller presented, which is 4.2 higher. Furthermore, as predicted by Fig.3.5, the presented controller has a speed extension ratio higher than double the single drive ($9.2\ p.u > (4 \times 2)\ p.u$), whereas the UPF controller has a speed extension ratio lower than double the single inverter drive ($5\ p.u < (4 \times 2)\ p.u$). Moreover, such a high speed extension ratio, 9.2 p.u, has been achieved by better utilization of the existing supplies without adding extra hardware or increasing the system rating compared to UPF DID.

The operating point where the single DC power supply DID starts to behave the same as the presented scheme is defined as point H in Fig.5.10a. At that point, both the presented and the single DC-link schemes have the same drive output power, torque, and per-unit speed. After which, the presented scheme has the advantage over the single DC-link DID with higher output mechanical power and a speed extension ratio of 9.2 compared to 8.4 for the single DC-link DID.

Three drive configurations have a speed extension ratio higher than double the single drive, which are presented, single DC power supply, and two isolated DC power supplies DIDs,

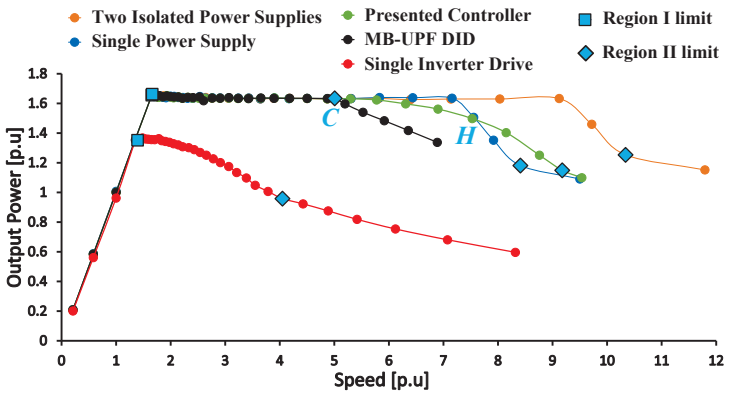

(a)

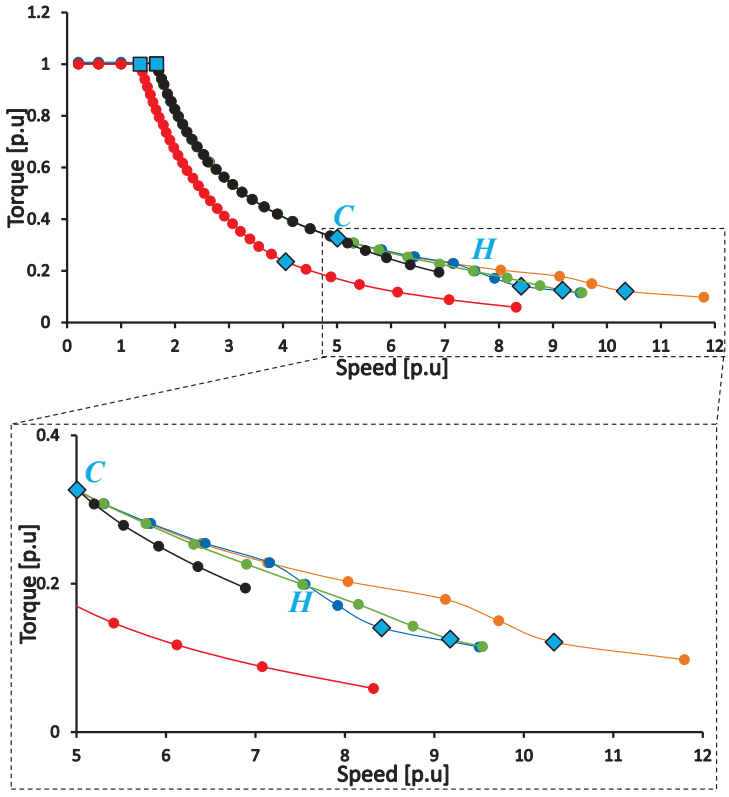

(b)

Figure 5.10: Experimental steady state behavior of the five drives. (a) Output steady state power curves, and (b) steady state torque curves.

whereas one drive configuration, which is UPF DID, has a speed extension ration lower than double the single inverter drive.

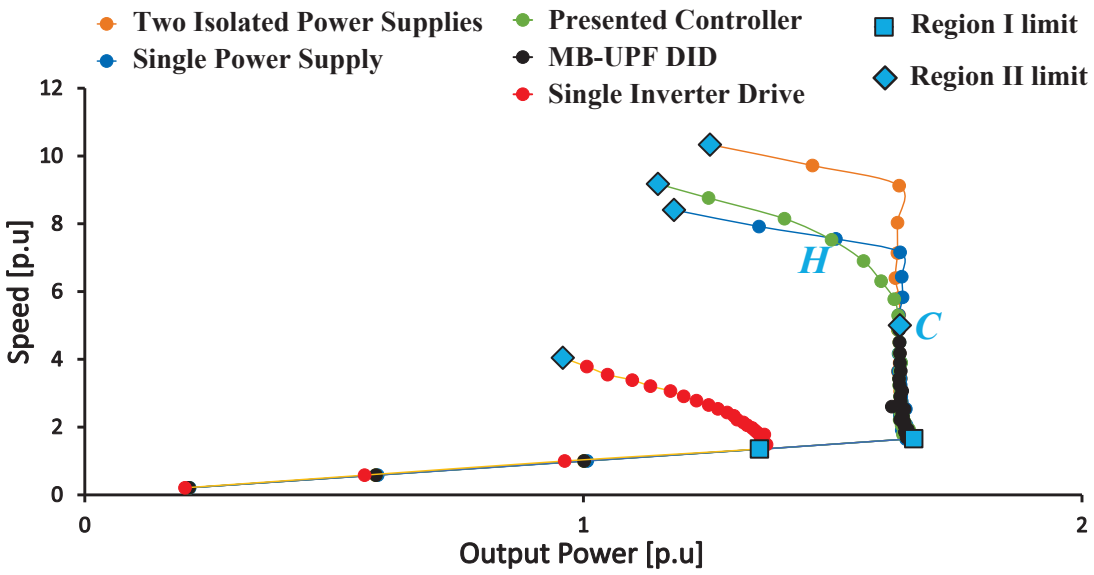

Figure 5.11: Experimental power steady state behaviour of five drives.

As described before[6], the speed is a function of the reactive voltage (reactive power), whereas the output power is a function of the active voltage (active power). Then re-plotting Fig.5.10a so that the output power (active voltage) is in X-axis, whereas the speed (reactive voltage) is in Y-axis, we will get a figure similar to that of Fig.3.5, see Fig.5.11. This better shows point C, point H, and the performance of the presented controller compared to the other drives and supports the discussion of Fig.5.10a.

Fig.5.12 shows the experimental simultaneous waveforms of the MB fundamental phase voltage, the FB fundamental phase voltage, and the motor phase current to verify the MB UPF operation, the MB non-UPF operation, and the FB reactive power support. As can be seen from Fig.5.12a, the MB fundamental phase voltage is in phase with the motor phase current, which means the MB is operated at UPF and only the FB is supplying the motor reactive power demand, FB fundamental phase voltage is 90° leading the motor phase current. Furthermore, the phase shift between the MB and FB fundamental voltages is 90°, see Fig.5.12a. Once the FB reaches its limit, the MB is then used to supply some reactive demand. The MB voltage is leading the motor phase current and the phase between the MB and FB voltage is $< 90°$, which means the MB is operated at non-UPF, see Fig.5.12b.

[6]See Chapter 2.

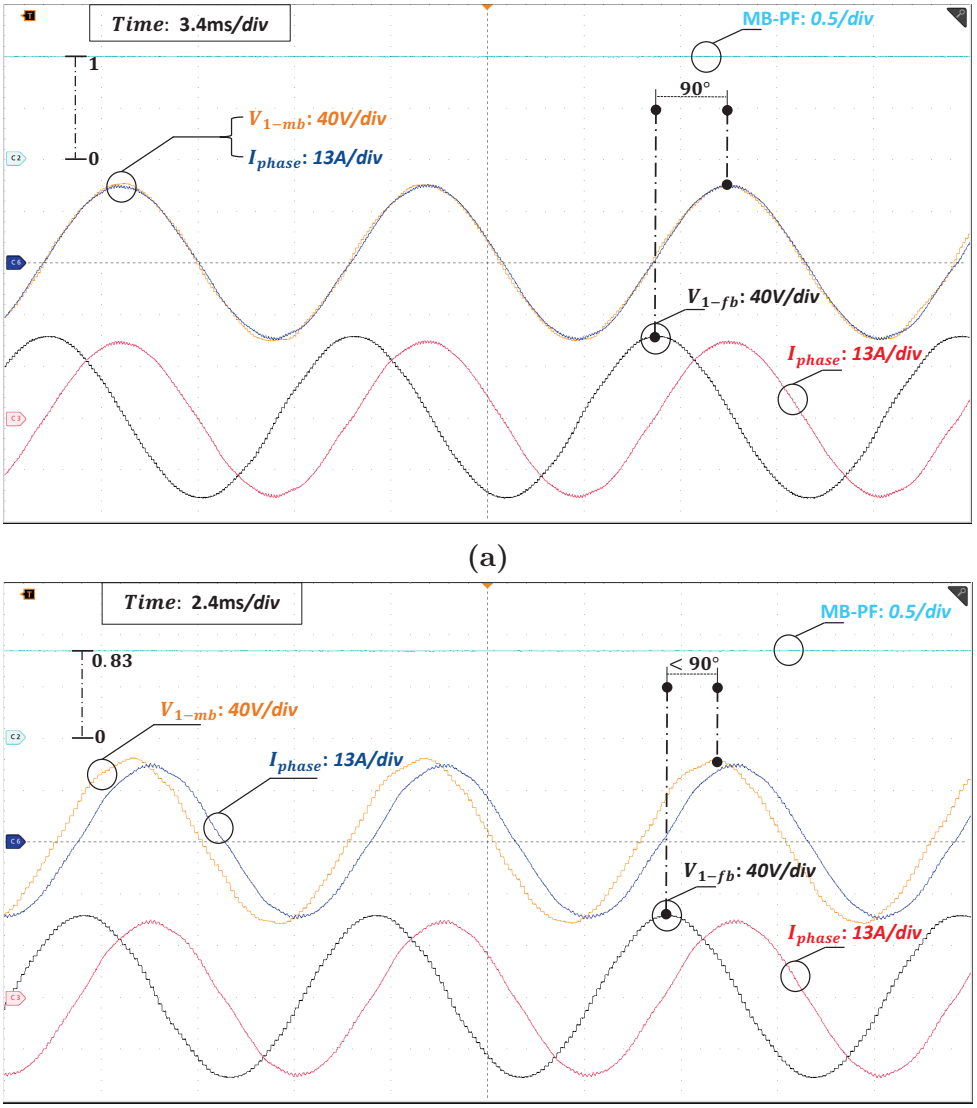

Figure 5.12: MB PF and simultaneous waveforms of the MB fundamental phase voltage, the FB fundamental phase voltage, and the motor phase current. (a) MB UPF operation, (b) MB non-UPF operation (MB-PF $\cong$ 0.83).

5.2.3 Maximum Fundamental Stator Voltage Comparison

Fig.5.13 compares the experimental maximum fundamental stator voltage of the single inverter drive, presented and UPF DIDs as a function of single inverter drive maximum fundamental voltage. As can be seen, the maximum fundamental voltage applied to IM stator is 1.82 for the controller presented, whereas it is 1.3 for UPF DID, which is 0.52

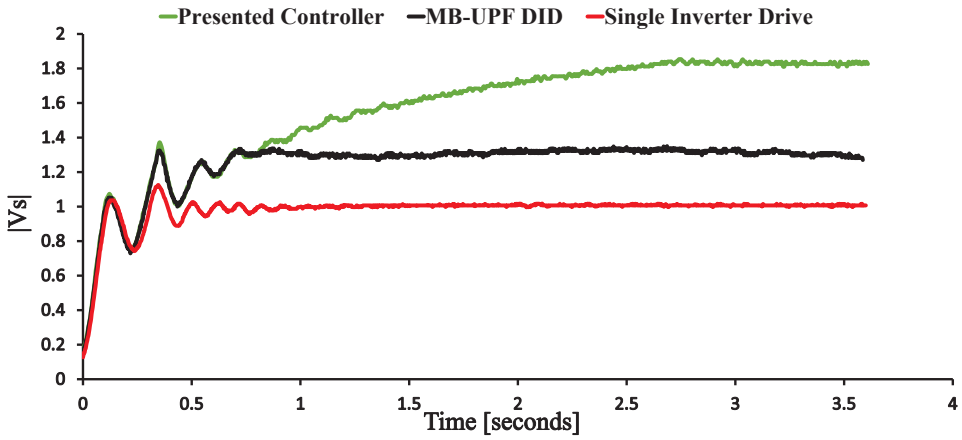

Figure 5.13: Experimental maximum stator voltage.

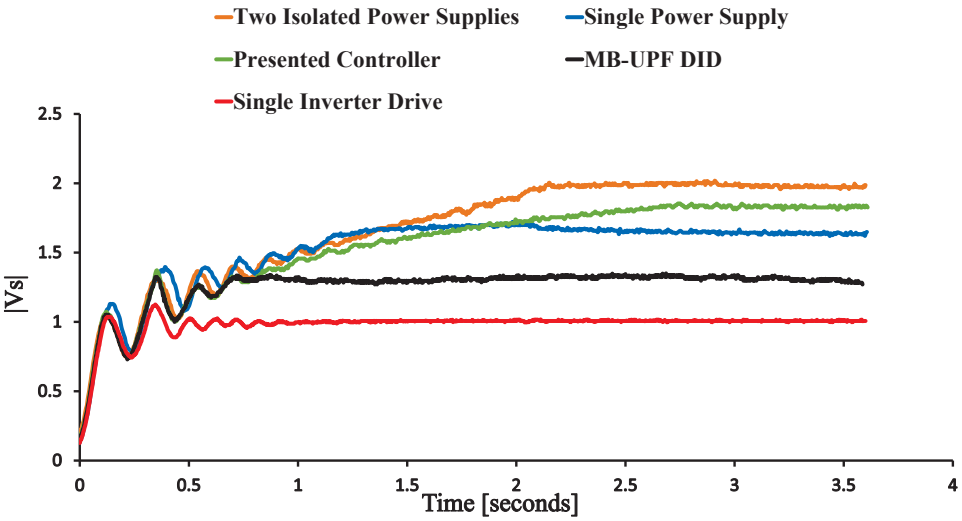

Figure 5.14: Experimental maximum stator voltage comparison.

higher. This means that for the same DC-link voltage, the presented controller better utilizes the system supplies than UPF DID. As a result, a DC-link voltage ratio of 1:2 is not necessary with the presented controller as it can increase the DC-link voltage utilization and boost the fundamental voltage up to 1.82 p.u., which is close to that achieved by two isolated DC power supplies DID (2 p.u.).

Boosting the fundamental stator voltage from 1.3 p.u (of UPF DID) to 1.82 p.u (of the presented controller) has been achieved without adding extra hardware or increasing the system rating. The DC-link voltage of both the MB and the FB can be reduced by 26% [13] with the presented controller, which means lower inverter power losses, less stresses

on the motor winding, lower dv/dt, lower battery DC voltage, and lower switches rating. The speed extension ratio after lowering the DC-link voltage by 26% is nearly about 6.2 p.u, which still higher than the speed extension ratio of UPF DID that uses 26% higher DC-link voltage.

A comparison of the five drive configurations maximum fundamental stator voltage is shown in Fig.5.14. The maximum stator voltage of each drive is per-unitized by the single inverter drive maximum fundamental voltage (V_m). As can be seen, the presented controller maximum voltage is 0.82 p.u, 0.52 p.u, and 0.16 p.u higher compared to the single inverter drive, MB-UPF, and single DC power supply DIDs, respectively, and only 0.17 p.u lower than that of two isolated DC power supplies DID. This explains why the speed extension ratio of the presented controller is higher than MB-UPF and single DC power supply DIDs and really close to two isolated DC power supplies DID.

5.2.4 Speed Acceleration Comparison

The experimental speed acceleration comparison of three drive configurations is shown in Fig.5.15a. The speed acceleration behavior follows the steady state behavior. The presented and MB-UPF controllers have the same acceleration time until a specific point, which can be defined as point C of Fig.5.10a. After which, the controller presented has higher P_{mech}, see Fig.5.10a, hence it has a higher acceleration than MB-UPF controller. For a speed step of 4000 rpm, the controller presented reaches the reference speed 2 seconds faster than the MB-UPF control. Moreover, for a speed step to 3500 rpm, the presented controller reaches the reference speed 2.8 seconds faster than the single inverter drive control.

The speed acceleration behaviour of the single DC power supply is similar to that of presented controller, see Fig.5.15b. It has a slightly better speed acceleration between t=1-2 sec because it has a higher output mechanical power than the presented controller, Fig.5.10a and Fig.5.15b. After t=2 sec, the presented controller has slightly higher output mechanical power and hence better speed acceleration.

The two isolated DC power supplies has the best acceleration performance among all five drives, see Fig.5.15c, since it has two DC power supplies and the highest output mechanical power compared to the other drives.

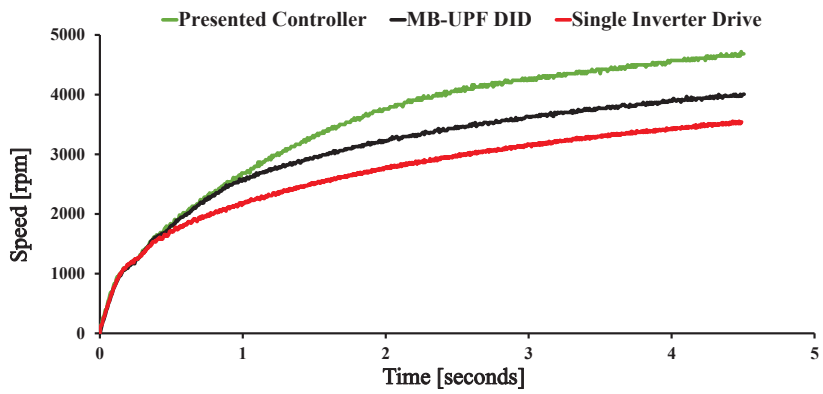

(a)

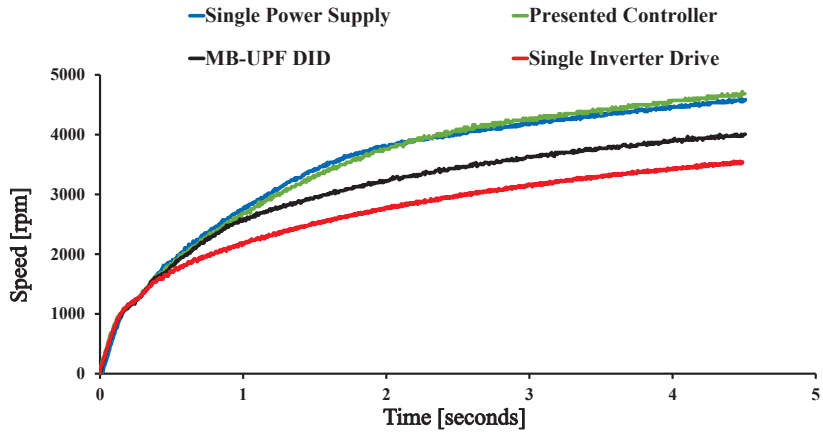

(b)

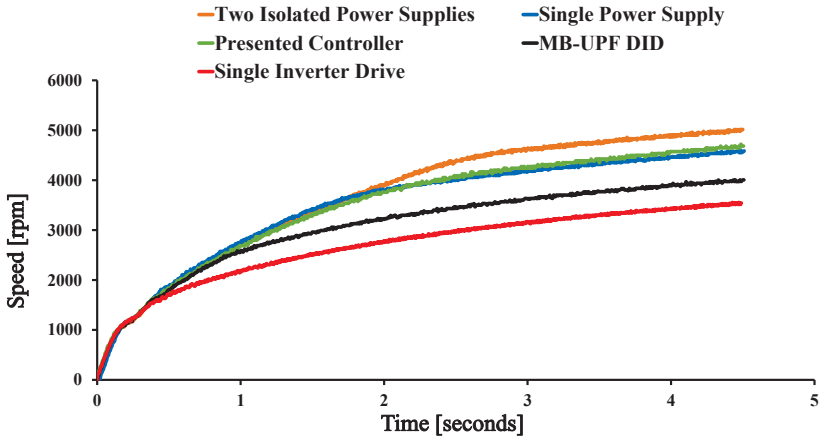

(c)

Figure 5.15: Experimental speed acceleration comparison of the presented controller with: (a) First two drives, (b) first two drives and single DC power supply DID, and (c) all drives.

Table 5.2: Different drives performance comparison.

Drive Configuration	**Single drive**	**MB UPF**	**Presented Work**	**Single DC supply**	**Two DC supplies**
Region I speed limit (ω_1/ω_{rated})	1.3	1.7	1.7	1.7	1.7
Speed Extension Ratio (ω_2/ω_{rated})	4	5	9.2	8.4	10.3
Torque Capability [p.u.]	0.07	0.19	0.226	0.228	0.228
Power Capability [p.u.]	0.7	1.3	1.6	1.64	1.64
Max. Fundamental Stator Voltage [p.u.]	1	1.3	1.82	1.66	2

Table 5.2 summarizes the different drive configurations in terms of Region I speed limit, speed extension ratio, electromechanical torque, output mechanical power, and maximum stator voltage. The speed limit, electromechanical torque, output mechanical power, and maximum stator voltage are per-unitized by base values ω_{rated}, $T_{e,rated}$, $P_{mech,rated}$, and $|V_m|$, respectively. The output drive torque and power capabilities are measured at a speed of 6.9 [p.u].

5.3 Potential DID Efficiency Improvement

The FB DC-link voltage is assumed constant in all operating conditions in the paper. However, this FB DC-link voltage can be variable and optimized in a manner to improve the overall drive efficiency. Since with the presented approach, the IM demand is decoupled into active and reactive components, it is possible to always monitor the IM reactive demand and based on it changing the FB DC-link voltage.

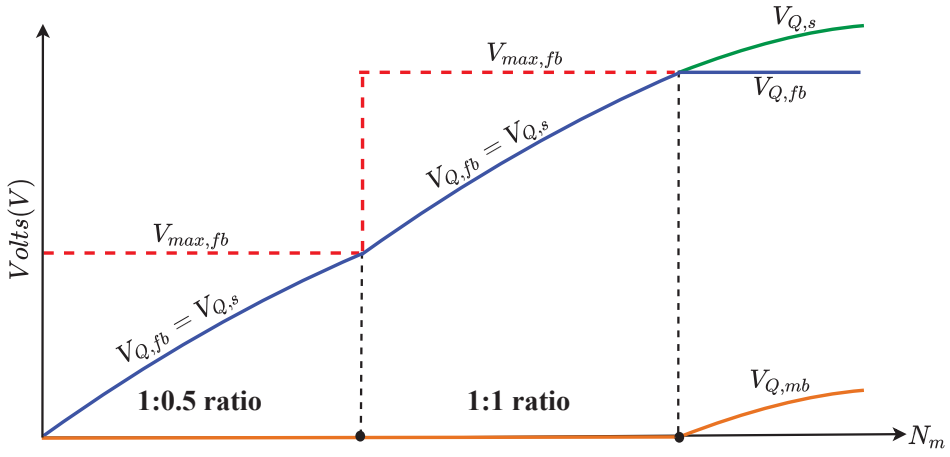

Figure 5.16: Stages of supplying reactive demand with first approach.

5.3.1 First Approach

As demonstrated in the paper, the motor reactive demand is fully supplied by the FB until it's maximum limit is reached and then the MB is used to supply some reactive demand.

For simplicity, if the capacitor is assumed ideal and at steady state, then

$$V_{P,fb} = 0 \tag{5.1}$$

and

$$|\overline{v}_{fb}| = v_{Q,fb} \tag{5.2}$$

Initially, the MB:FB DC-link voltage ratio is 1:0.5. As the motor speed increases, the reactive demand of the motor increases until $v_{Q,s} = V_{max,fb}$ and then the DC-link voltage ratio is increased to 1:1. If the motor speed is increased more, the motor reactive demand increases more until $v_{Q,s} = V_{max,fb}$, and then the MB is used to supply some reactive demand, see Fig.5.16.

The advantage of this is that by making the FB DC-link voltage variable, in this example only between two DC-link voltage ratios, the DID performance is better in terms of FB switching power losses (it is lower by 50% when the DC-link voltage ratio is 1:0.5), and FB switches voltage stress. However, instead of changing the FB DC-link voltage only

between two values, it can be variable with the actual motor state, which will further improve the drive efficiency.

5.3.2 Second Approach

At low torque values, the active motor power demand supplied by the MB is low. Hence, at low torque values, the MB capacity is not fully used to supply active motor demand. With the first approach, the FB full capacity is first used to supply reactive demand and then the MB is used to supply some reactive demand. Unlike the first approach, the second approach uses the MB underutilized capacity in supplying active demand, to supply some reactive demand before the FB reaches its maximum.

The motor is operated at the rated speed while applying the rated torque and then at t=3 sec, the applied torque is reduce from 1 p.u. to almost 0.1 p.u., Fig.5.17a. As a result, the motor active voltage demand decreases, whereas reactive voltage demand increases, Fig.5.17b, Fig.5.17c, and Fig.5.17d. If first approach is applied, as the reactive voltage demand increases, the FB DC-link voltage is increased from 0.84 p.u. to 1 p.u. to supply that demand, Fig.5.17e. The MB supplied active voltage is decreased from 0.93 p.u. to 0.22 p.u., Fig.5.17c, which means that there is an underutilized MB capacity before and after changing the load.

If the second approach is applied, the MB is used to supply some reactive demand before the load change and the modulation index of the MB is maximized to the maximum. This reduces the FB DC-link voltage from 0.84 p.u. (first approach) to 0.48 p.u. (second approach), Fig.5.18e. Furthermore, with the second approach, the increment in FB DC-link voltage after changing the load has been avoided and the capacitor DC-link voltage is even reduced more, which further improves the drive efficiency, Fig.5.18.

However, the focus of this paper is to present a FW controller that extends the speed range of a DID with a FB. The efficiency improvement is a potential future work and has not been discussed for all operating conditions or implemented in this thesis work.

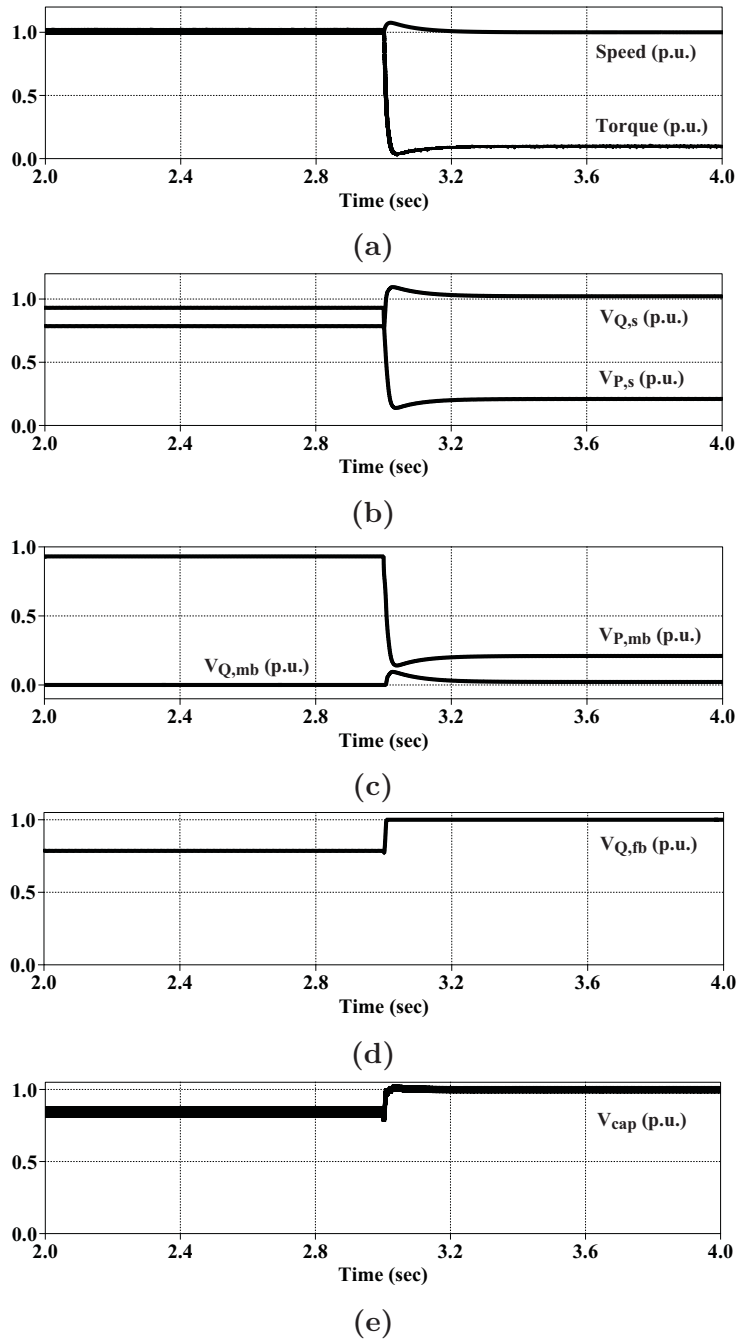

Figure 5.17: Drive efficiency improvement using the first approach: (a) Torque and speed curves, (b) active and reactive stator demand, (c) active and reactive demand supplied by MB, (d) reactive demand supplied by FB, (e) FB DC-link voltage.

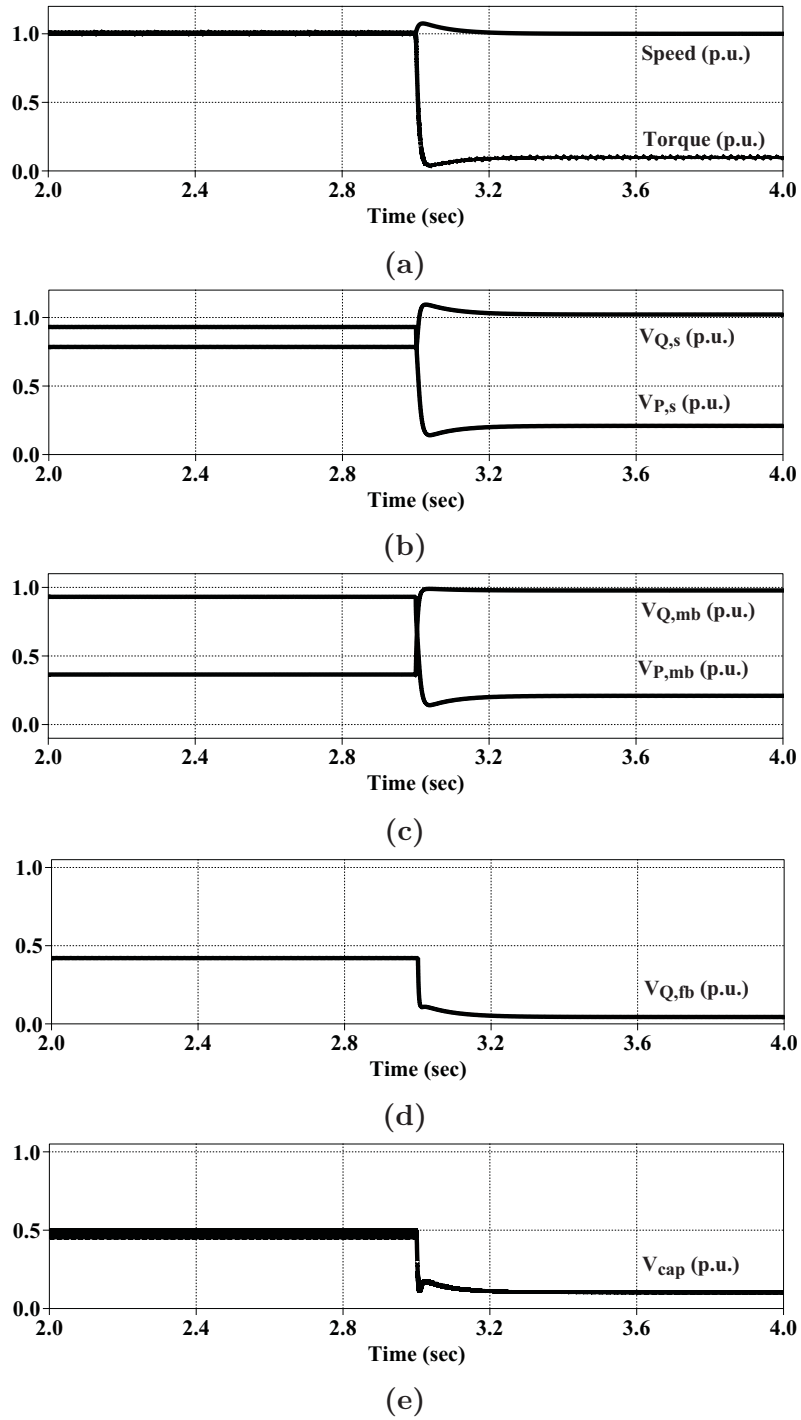

Figure 5.18: Drive efficiency improvement using the second approach: (a) Torque and speed curves, (b) active and reactive stator demand, (c) active and reactive demand supplied by MB, (d) reactive demand supplied by FB, (e) FB DC-link voltage.

5.4 Summary

A new field weakening control scheme for the DID using an OEWIM with a floating capacitor bridge is presented and its experimental results are compared with other four field weakening control schemes, three of which are DID schemes. The contribution of the presented FW scheme can be summarized as follows.

- At low speeds, the main bridge connected to the main power source is operated at UPF, whereas the motor reactive power demand is fully supplied by the floating capacitor bridge.
- At high speeds, the main bridge is used to supply some reactive power demand after the floating bridge reaches a maximum limit to extend the field weakening region. As a result, the field weakening region is extended to 9.2 per-unit speed compared to 5 per-unit speed when always operating the main bridge at UPF.
- The presented field weakening scheme maintains the features of the UPF DID described in literature up to a specific per-unit speed and boosts the drive's output power and speed performance after.
- The single DC supply DID at a specific per-unit speed output the same mechanical power as the presented scheme. After which, the presented scheme has the advantage and boosts both the motor speed and output mechanical power.
- The speed extension ratio of the presented work (9.2 p.u) is higher than double the speed extension ratio of the single inverter drive (4 p.u).
- The maximum fundamental voltage of the work presented is 1.82 p.u when compared to single inverter drive maximum voltage.

The basic principle of how the dual inverter drive using a floating capacitor bridge efficiency can be improved by operating the main bridge at non-UPF is also presented. The drive efficiency can be improved at low and high torque values, with the improvement being more prominent at low torque values.

Chapter 6

Conclusion

High speed machines are required for applications, such as, spindle, servo, and electric vehicles. The induction motor is the considered choice due to its high reliability and wide speed operating range that can be achieved easily by means of a field weakening control scheme.

The field weakening operation of an induction motor means that the motor speed can be increased above its rated base speed by weakening the motor flux. The flux level can be adjusted by the voltage closed loop field adjusting method, which is the most common method and the one adopted in this work, where the flux is weakened based on the voltage requested by the motor.

There are three operating regions when it comes to field weakening operation of a motor. These regions are the constant torque region, field weakening region, and decreasing power region. Furthermore, it is always desirable to retain the maximum output torque and power capability of a machine during all operating regions under the current and voltage constraints. These operating regions, voltage and current constraints are described in Chapter 1.

Dual inverter drives using open-ended winding induction machines can be used to boost the motor voltage compared to a single inverter drive. The open-ended winding induction machine can be connected to a DC power supply and a floating capacitor bridge, to two isolated DC power supplies, or to a single DC power source.

The floating capacitor bridge drive, which is the one adopted and improved in this work, has recently gained popularity as it not only eliminates common-mode circulating current

paths, but also reduces the drive size, weight, and cost as well as the need for a common-mode reactor.

The motor reactive power requirement (VArs) is supplied by the floating bridge, whereas the main bridge is operated at unity power factor until the floating bridge reaches its maximum fundamental voltage limit. After which, the main bridge is used to supply some reactive demand to further extend the field weakening region. The mathematical model of the floating capacitor bridge, constant torque, field weakening, and decreasing power regions speed limit of the presented work are described in Chapter 2. The voltage boundary limits of five drives, including the presented work, that can be used to predict the drive's performance in the field weakening region are also described in Chapter 2. It has been shown that in order to boost the output mechanical power, the active power supplied to the motor need to be boosted. The active power is mainly a function of active voltage. It has also been shown that the field weakening region can be extended by supplying more reactive voltage. Since the presented controller can operate the main bridge at non-UPF to supply some reactive demand, it can extend the field weakening region over the DID that restricts the main bridge operation only at UPF.

The motor demand can be decoupled into active and reactive components by introducing a second reference frame, the stator current reference frame, in addition to the rotor flux reference frame. The latter is used in this work to separate the stator current into torque and field current components. The stator current reference frame simplifies the control of both the main bridge and floating bridge and adds more flexibility for the real and reactive power control of both bridges. Most significantly for the work presented, this reference frame allows the main bridge to supply some reactive power at high speeds.

The presented work control scheme is described in Chapter 4, along with the stator current reference frame and the field weakening limits that are used to transfer from one operating region to another. The field weakening controllers of the single inverter drive, main bridge UPF, single DC power supply, and two isolated DC power supplies are also presented in Chapter 4.

The simulation and experimental waveforms presented in Chapter 5 show that the speed extension ratio of the controller presented is 5.2, 4.2, and 0.8 higher when compared to single inverter drive, main bridge UPF, and single DC power supply dual inverter drives. The two isolated DC power supplies dual drive has a 1.1 p.u higher speed extension

ratio when compared with the presented controller. Furthermore, the presented controller retains the same features of the UPF dual drive until a specific operating point and extends both the drive output power, and torque over the UPF drive after that point.

The experimental results show that the presented controller also accelerates the motor to high speeds faster than single inverter and main bridge UPF drives and gives a maximum fundamental voltage that is 0.82 p.u, 0.52 p.u., and 0.16 p.u. higher compared to single inverter drive, main bridge UPF and single power supply dual inverter drives, respectively, and only 0.17 p.u. lower than that of two isolated power supplies.

Boosting the fundamental stator voltage by 0.52 p.u. over the main bridge UPF dual inverter drive has been achieved without adding extra hardware or increasing the system rating, which adds additional feature to the presented work. The DC-link voltage of both the main bridge and the floating bridge can be reduced by 26% and the speed extension ratio is still higher than that of UPF dual drive that uses 26% higher DC-link voltage.

Bibliography

[1] S. Wdaan, C. Perera and J. Salmon, "Maximum Torque Operation of Open-Winding Induction Motor Dual Drives Using a Floating Capacitor Bridge in the Field Weakening Region," in IEEE Transactions on Power Electronics, vol. 37, no. 8, pp. 9629-9640, Aug. 2022.

[2] Veltman, A., Pulle, D. W., & De Doncker, R. W. (2007). Fundamentals of electrical drives (Vol. 345). Power systems: Springer.

[3] B. M. Wilamowski, J. Irwin, Power Electronics and Motor Drives (The Industrial Electronics Handbook), FL, Boca Raton:CRC Press, 2011.

[4] Z. Zhang, Y. Liu and A. M. Bazzi, "An improved high-performance open-loop V/f control method for induction machines," 2017 IEEE Applied Power Electronics Conference and Exposition (APEC), 2017, pp. 615-619, doi: 10.1109/APEC.2017.7930757.

[5] Automation, R. O. C. K. W. E. L. L. (2000). AC Drives Using PWM Techniques. USA: DRIVESWP002A-EN-P.

[6] Yu, J., Zhang, T., & Qian, J. (2011). Modern control methods for the induction motor, electrical motor products. Electrical Motor Products: International Energy-Efficiency Standards and Testing Methods, 147-172.

[7] Amirnaser Yazdani; Reza Iravani, "Variable-Frequency VSC System," in Voltage-Sourced Converters in Power Systems: Modeling, Control, and Applications , IEEE, 2010, pp.270-310, doi: 10.1002/9780470551578.ch10.

[8] D. Casadei, M. Mengoni, G. Serra, A. Tani and L. Zarri, "A Control Scheme With Energy Saving and DC-Link Overvoltage Rejection for Induction Motor Drives of Electric Vehicles," in IEEE Transactions on Industry Applications, vol. 46, no. 4, pp. 1436-1446, July-Aug. 2010.

[9] B. Wang, J. Zhang, Y. Yu, X. Zhang and D. Xu, "Unified Complex Vector Field-Weakening Control for Induction Motor High-Speed Drives," in IEEE Transactions on Power Electronics, vol. 36, no. 6, pp. 7000-7011, June 2021.

[10] Sang-Hoon Kim and Seung-Ki Sul, "Voltage control strategy for maximum torque operation of an induction machine in the field-weakening region," in IEEE Transactions on Industrial Electronics, vol. 44, no. 4, pp. 512-518, Aug. 1997.

[11] Sang-Hoon Kim and Seung-Ki Sul, "Maximum torque control of an induction machine in the field weakening region," in IEEE Transactions on Industry Applications, vol. 31, no. 4, pp. 787-794, July-Aug. 1995.

[12] J. Ewanchuk and J. Salmon, "A Square-wave Controller for a high speed induction motor drive using a three phase floating bridge inverter," 2010 IEEE Energy Conversion Congress and Exposition, Atlanta, GA, 2010, pp. 2584-2591.

[13] C. Perera, G. J. Kish and J. Salmon, "Decoupled Floating Capacitor Voltage Control of a Dual Inverter Drive for an Open-Ended Winding Induction Motor," in IEEE Transactions on Power Electronics, vol. 35, no. 7, pp. 7305-7316, July 2020.

[14] M. Mengoni, L. Zarri, A. Tani, G. Serra and D. Casadei, "Stator Flux Vector Control of Induction Motor Drive in the Field Weakening Region," in IEEE Transactions on Power Electronics, vol. 23, no. 2, pp. 941-949, March 2008.

[15] Seung-Ki Sul, "Vector Control [1 and 2]," in Control of Electric Machine Drive Systems , IEEE, 2011, pp.230-282.

[16] Z. Dong, Y. Yu, W. Li, B. Wang and D. Xu, "Flux-Weakening Control for Induction Motor in Voltage Extension Region: Torque Analysis and Dynamic Performance Improvement," in IEEE Transactions on Industrial Electronics, vol. 65, no. 5, pp. 3740-3751, May 2018.

[17] H. Stemmler and P. Guggenbach, "Configurations of high-power voltage source inverter drives," 1993 Fifth European Conference on Power Electronics and Applications, Brighton, UK, 1993, pp. 7-14 vol.5.

[18] J. S. Park and K. Nam, "Dual Inverter Strategy for High Speed Operation of HEV Permanent Magnet Synchronous Motor," Conference Record of the 2006 IEEE Industry Applications Conference Forty-First IAS Annual Meeting, 2006, pp. 488-494.

[19] R. U. Haque, M. S. Toulabi, A. M. Knight and J. Salmon, "Wide speed range operation of PMSM using an open winding and a dual inverter drive with a floating bridge," 2013 IEEE Energy Conversion Congress and Exposition, 2013, pp. 3784-3791.

[20] Y. Lee and J. Ha, "Power enhancement of dual inverter for open-end permanent magnet synchronous motor," 2013 Twenty-Eighth Annual IEEE Applied Power Electronics Conference and Exposition (APEC), 2013, pp. 1545-1551.

[21] Z. Shen, D. Jiang, J. Chen and R. Qu, "A novel zero-sequence current elimination PWM scheme for an open-end winding motor drive with dual two-level inverter," 2018 IEEE Applied Power Electronics Conference and Exposition (APEC), San Antonio, TX, 2018, pp. 1679-1686.

[22] Akihito Mizukoshi, Hitoshi Haga, Reduction of Voltage Harmonics in an Open-End Winding Induction Motor Driven by a Dual-Inverter with a Floating Capacitor in a Partial-Load Condition, IEEJ Journal of Industry Applications, 2021, Volume 10, Issue 5, Pages 564-574.

[23] Z. Huang, T. Yang, P. Giangrande, S. Chowdhury, M. Galea and P. Wheeler, "Enhanced Performance of Dual Inverter With a Floating Capacitor for Motor Drive Applications," in IEEE Transactions on Power Electronics, vol. 36, no. 6, pp. 6903-6916, June 2021.

[24] V. T. Somasekhar, S. Srinivas, B. P. Reddy, C. N. Reddy and K. Sivakumar, "Pulse width-modulated switching strategy for the dynamic balancing of zero-sequence current for a dual-inverter fed open-end winding induction motor drive," in IET Electric Power Applications, vol. 1, no. 4, pp. 591-600, July 2007.

[25] M. R. Baiju, K. K. Mohapatra, R. S. Kanchan and K. Gopakumar, " A dual two-level inverter scheme with common mode voltage elimination for an induction motor drive," in IEEE Transactions on Power Electronics, vol. 19, no. 3, pp. 794-805, May 2004.

[26] A. Edpuganti and A. K. Rathore, "New Optimal Pulsewidth Modulation for Single DC-Link Dual-Inverter Fed Open-End Stator Winding Induction Motor Drive," in IEEE Transactions on Power Electronics, vol. 30, no. 8, pp. 4386-4393, Aug. 2015.

[27] H. Kubo, Y. Yamamoto, T. Kondo, K. Rajashekara and B. Zhu, "Zero-sequence current suppression for open-end winding induction motor drive with resonant controller," 2016 IEEE Applied Power Electronics Conference and Exposition (APEC),

Long Beach, CA, 2016, pp. 2788-2793.

[28] D. Casadei, G. Grandi, A. Lega and C. Rossi, "Multilevel Operation and Input Power Balancing for a Dual Two-Level Inverter with Insulated DC Sources," in IEEE Transactions on Industry Applications, vol. 44, no. 6, pp. 1815-1824, Nov.-dec. 2008.

[29] E. G. Shivakumar, K. Gopakumar, S. K. Sinha, A. Pittet and V. T. Ranganathan, "Space vector PWM control of dual inverter fed open-end winding induction motor drive," APEC 2001. Sixteenth Annual IEEE Applied Power Electronics Conference and Exposition (Cat. No.01CH37181), Anaheim, CA, USA, 2001, pp. 399-405 vol.1.

[30] Junha Kim, Jinhwan Jung and Kwanghee Nam, "Dual-inverter control strategy for high-speed operation of EV induction motors," in IEEE Transactions on Industrial Electronics, vol. 51, no. 2, pp. 312-320, April 2004.

[31] M. Mengoni, A. Amerise, L. Zarri, A. Tani, G. Serra and D. Casadei, "Control Scheme for Open-Ended Induction Motor Drives With a Floating Capacitor Bridge Over a Wide Speed Range," in IEEE Transactions on Industry Applications, vol. 53, no. 5, pp. 4504-4514, Sept.-Oct. 2017.

[32] S. Singh, C. Perera, G. J. Kish and J. Salmon, "PWM Control of a Dual Inverter Drive using a Floating Capacitor Inverter," 2019 20th Workshop on Control and Modeling for Power Electronics (COMPEL), Toronto, ON, Canada, 2019, pp. 1-8.

[33] A. Amerise, M. Mengoni, L. Zarri, A. Tani, S. Rubino and R. Bojoi, "Open-End Windings Induction Motor Drive With Floating Capacitor Bridge at Variable DC-Link Voltage," in IEEE Transactions on Industry Applications, vol. 55, no. 3, pp. 2741-2749, May-June 2019.

[34] Y. Jia et al., "Control Strategy for an Open-End Winding Induction Motor Drive System for Dual-Power Electric Vehicles," in IEEE Access, vol. 8, pp. 8844-8860, 2020.

[35] M. Darijevic, M. Jones, O. Dordevic and E. Levi, "Decoupled PWM Control of a Dual-Inverter Four-Level Five-Phase Drive," in IEEE Transactions on Power Electronics, vol. 32, no. 5, pp. 3719-3730, May 2017.

[36] V. T. Somasekhar, K. Gopakumar, A. Pittet and V. T. Ranganathan, "PWM inverter switching strategy for a dual two-level inverter fed open-end winding induction motor

drive with a switched neutral," in IEE Proceedings - Electric Power Applications, vol. 149, no. 2, pp. 152-160, March 2002.

[37] I. J. Smith and J. Salmon, "High-Efficiency Operation of an Open-Ended Winding Induction Motor Using Constant Power Factor Control," in IEEE Transactions on Power Electronics, vol. 33, no. 12, pp. 10663-10672, Dec. 2018.

[38] D. Gerada, A. Mebarki, N. L. Brown, C. Gerada, A. Cavagnino and A. Boglietti, "High-Speed Electrical Machines: Technologies, Trends, and Developments," in IEEE Transactions on Industrial Electronics, vol. 61, no. 6, pp. 2946-2959, June 2014.

[39] R. Abebe, M. Di Nardo, D. Gerada, G. L. Calzo, L. Papini and C. Gerada, "High speed drives review: Machines, converters and applications," IECON 2016 - 42nd Annual Conference of the IEEE Industrial Electronics Society, 2016, pp. 1675-1679.

[40] A. Amerise, M. Mengoni, G. Rizzoli, L. Zarri, A. Tani and G. Serra, "Open-End Winding Induction Motor Drive with a Floating Capacitor Bridge and Overmodulation of the Primary Inverter," 2018 IEEE Energy Conversion Congress and Exposition (ECCE), 2018, pp. 2394-2400.

[41] Nisha G.K., Lakaparampil Z.V. and Ushakumari S., "Four-quadrant operation of sensorless FOC induction machine in field weakening region using MRAS-sliding mode observer," 2013 International Conference on Control Communication and Computing (ICCC), 2013, pp. 33-38, doi: 10.1109/ICCC.2013.6731620.

[42] X. Sun, Z. Liu, D. Jiang and W. Kong, "Multiphase Open-End Winding Induction Machine Drive With the Floating Capacitor," in IEEE Transactions on Industry Applications, vol. 56, no. 5, pp. 5013-5022, Sept.-Oct. 2020.